isvr Institute of Sound and Vibration Research

Use of Cross-Correlation for Leak Detection in Plastic Pipes

Y.Gao, M.J. Brennan, P.F. Joseph and J.M. Muggleton

ISVR Technical Memorandum No 901

December 2002

University of Southampton

SCIENTIFIC PUBLICATIONS BY THE ISVR

Technical Reports are published to promote timely dissemination of research results by ISVR personnel. This medium permits more detailed presentation than is usually acceptable for scientific journals. Responsibility for both the content and any opinions expressed rests entirely with the author(s).

Technical Memoranda are produced to enable the early or preliminary release of information by ISVR personnel where such release is deemed to the appropriate. Information contained in these memoranda may be incomplete, or form part of a continuing programme; this should be borne in mind when using or quoting from these documents.

Contract Reports are produced to record the results of scientific work carried out for sponsors, under contract. The ISVR treats these reports as confidential to sponsors and does not make them available for general circulation. Individual sponsors may, however, authorize subsequent release of the material.

UNIVERSITY OF SOUTHAMPTON

INSTITUTE OF SOUND AND VIBRATION RESEARCH

DYNAMICS GROUP

Use of Cross-Correlation for Leak Detection in Plastic Pipes

by

Y. Gao, M.J. Brennan, P.F. Joseph and J.M. Muggleton

ISVR Technical Memorandum No: 901

December 2002

Authorised for issue by
Professor M.J. Brennan
Group Chairman

Abstract

Water leaks are a topic of great concern in Britain and many other countries, because of decreasing water supplies and the deterioration of old pipework. In leak detection surveys, the most widely used technique for many years has been the cross-correlation technique. Currently plastic pipes are used in most water distribution networks due to low cost and their easy handling characteristics. However in many practical situations, the application of correlation techniques for plastic pipes involves several factors, including background noise, acoustic wave attenuation in the pipe and accessibility for sensors.

This report uses an analytical model of a buried plastic pipe to investigate the effectiveness of the cross-correlation technique in water leak detection. Based on the fact that the fluid-borne axisymmetric wavenumber increases monotonically with frequency, an analytical model of propagation wavespeed and wave attenuation has been established in previous work. Assuming that the leak signal is band-limited white noise, an analytical model of the cross-correlation function for wave propagation in a pipe is established. It is found that the cross-correlation function is mainly dominated by the lower cut-off frequency provided that the bandwidth of the input white noise is relatively broad. The analytical models are validated using some experimental results provided by the National Research Council of Canada. The model of the correlation function provides an explanation for the effect of the filter cut-off frequencies used in the cross-correlation technique for leak detection.

Contents

1. Introduction

1.1 Introduction

Water leakage from buried pipes is a subject of great concern in Britain, and many other countries because of decreasing water supplies due to changing rainfall patterns, deterioration or damage to the distribution system, and an ever increasing population. Much attention has been paid to reducing water leakage over the past few years, since the loss of large amounts of water through faulty pipework system is environmentally and economically damaging.

An effective leak detection technique yields many benefits. First and foremost, there is an immediate saving in pumping and treatment production costs. Second, leaks discovered during a survey can be scheduled for repair, often eliminating the potential damage to the pipe network itself, e.g., major pipe breaks, and erosion of foundations of roads and buildings. In addition, by finding and fixing leaks, public health is protected as every leak is a potential entry point for contaminants if a pressure drop occurs in the system.

1.2 Literature review

1.2.1 Leak detection

A leak from a water supply pipe system generates noise, which can be used for leak detection and location. The effectiveness of the existing acoustic leak detection techniques and equipment has been demonstrated in the previous work [1-3]. Acoustic methods are commonly used to pinpoint leaks by most professional users. Other methods of leak detection which have been used with varying degrees of success are listening sticks, thermography [4], flow and pressure correlation, and ground penetrating radar (GPR) detection [5]. Each technique has both advantages and shortcomings. The potential of the non-acoustic technologies has been evaluated by Hunaidi et al [6, 7]. Although they show some promise, they are more complex and time-consuming, and may fail to detect leaks in practical conditions.

Generally leak detection using acoustic equipment is accomplished in two phases. During the first phase, the entire system is surveyed for leak sounds. An initial survey is usually conducted by listening devices such as listening sticks on all accessible contact points with the pipework system. When a sound is heard, the location is noted as a potential leak site. However, background noise may produce sounds with

characteristics similar to leak signals. During the second phase, each suspect location is further investigated. More accurate measurements can be taken to pinpoint the exact locations of the leaks by using geophones (or ground microphones) to listen for the leak sounds on the ground directly above the pipe at close intervals; or by using leak noise correlators.

Listening devices utilize sensitive mechanisms or materials, for example piezo-electric elements. Modern electronic devices may include signal amplifiers and noise filters, which could be very helpful in adverse environments. The use of listening sticks is straightforward, but the effectiveness depends on the experience of the user. On the other hand, a computerised leak correlator is used to pinpoint the exact location of the leak. The correlator eliminates the need for extensive hit-or-miss excavation, and the unnecessary destruction of expensive pavement. Normally a leak detection correlator is much more efficient and yields more accurate results compared to listening devices. Since the introduction of this device in the early 1980s, the correlation technique, which is the most widely used acoustic technique, has been significantly improved.

One of the reasons why the correlation technique is attractive for leak detection is its robustness in the presence of background noise [8]. For a given signal and noise situation, the cross-correlation can be used to improve the signal-to-noise ratio (SNR) by +3dB for every doubling of the integration period used. Especially for environments where a very poor SNR situation exists, increasing the length of time duration over which the cross-correlation is determined can reveal the presence of a previously masked signal.

Theoretically the cross-correlation technique is straightforward. The preliminary work is performed by measuring vibration or acoustic signals at two access points using vibration sensors such as accelerometers or hydrophones either side the location of a suspect leak. The signals from the sensors are transmitted in some manner to the leak noise correlator to pinpoint the leak. The noise correlator is a piece of equipment, which computes the cross-correlation function of the two signals and presents the results to an operator. The location of the leak relative to one of the measurement points is easily calculated using a simple algebraic relationship between the time shift of the peak value of the cross-correlation function, distance between the access points, and propagation wavespeed in the buried pipe.

Satisfactory results have been achieved when the correlation technique is applied to locate leaks in metal pipes. Currently plastic pipes made from PVC (polyvinylchloride) and MDPE (medium density polyethylene), are used in many water distribution networks due to low cost and their easy handling characteristics. However in many practical situations, the application of correlation techniques for plastic pipes involves several factors, including background noise, acoustic wave attenuation in the pipe and accessibility for sensors. The effectiveness of the existing technique for plastic pipe leak detection is not well established and most leak detection professionals are sceptical about locating leaks accurately. For the correlation technique to be effective, the propagation wavespeed must be known *a priori*. Relatively predictable for metal pipes, the acoustical characteristics of leak signals are largely unknown for the plastic pipe, as the wave propagation behaviour becomes highly coupled between the pipe wall and the contained fluid.

1.2.2 Wave propagation in pipes

Since current leak detection techniques rely on the vibration characteristics of pipework system, it is worthwhile to study these characteristics before investigating leak detection. The way in which vibration and waves propagate in thin-walled shells *in vacuo* and in fluid-filled elastic cylindrical ducts has been summarised by Fuller and Fahy [9, 10] by using fundamental equations from reference [11]. Some of the dispersion curves were experimentally confirmed by wavenumber spectra obtained from pipe surface acceleration measurements on a straight pipe [12]. The energy distribution among the various wave types was investigated theoretically for a radial wall input force and for internal pressure pulsations [13]. In these papers it was suggested that well below the pipe ring frequency four wave types are considered to be responsible for most of the energy transfer. These are three axisymmetric waves, with $n=0$, and the $n=1$ circumferential modes, which relate to beam bending. The first $n=0$ wave, termed $s=1$, is a predominantly fluid-borne wave, which is strongly influenced by the wall flexibility. The second wave, termed $s=2$, is predominantly the compressional wave in the shell with some associated radial wall motion influenced by the contained fluid. The third wave, $s=0$, is a torsional wave in the shell uncoupled from the contained fluid.

Experimental work carried out to validate the analytical perditions of axisymmetric wavespeed and attenuation for a fluid-filled elastic pipe *in vacuo* was provided by

Muggleton et al [14, 15]. More recently much attention has been focused on the characteristics of wave propagation in buried pipes in terms of the effect of the surrounding medium [16]. It is believed that the effect of the surrounding medium is to mass load the pipe and at low frequencies its effect on the axisymmetric wavenumbers is relatively small compared to the results for the fluid-filled pipe *in vacuo*.

For most practical pipework systems, leak detection is most successfully executed on low frequency leak signals, suggesting that waves propagate most effectively at these frequencies. In addition, recent work in Canada on typical PVC water distribution pipes [7, 17], has focused on the dominant low frequency signals. The acoustic characteristics of several types of realistic leaks simulated under controlled conditions were investigated, which confirmed that most leak noise energy is concentrated at low frequencies. The effectiveness of the cross-correlation technique was found to be largely affected by several considerations including the selection of vibration sensors and cut-off frequencies of high and low-pass digitised filters. Although it has been shown that leaks in plastic pipes can be located using the cross-correlation technique, little interpretation of the effect on cross-correlation functions is attempted in the literature.

1.3 Outline of report

The main body of this report consists of four sections. Following the introduction, an analytical model of the propagation wavespeed and wave attenuation is established in section 2. Assuming that the leak signal is band-limited white noise, an analytical model of the cross-correlation function is established. Several expressions for the theoretical predictions of cross-correlation functions including the cross-correlation coefficient are derived. The effect of the lower and upper cut-off frequencies of the leak signal on the theoretical results is also discussed. It is found that the cross-correlation function is mainly dominated by the lower cut-off frequency provided that the bandwidth of the input white noise is relatively broad.

In section 3 the analytical models are validated using some experimental results provided by the National Research Council of Canada. Good agreement has been achieved in the analysis of propagation wavespeed and attenuation in the buried fluid-filled pipe. Regarding the normalised cross-correlation functions calculated, the model presented is found to provide a reasonable explanation for the effect of the filter cut-off frequencies used in the cross-correlation technique for leak detection.

Finally, some conclusions are drawn in section 4. There are three Appendixes in this report. The dynamic behaviour of fluid-filled pipes *in vacuo* is reviewed in Appendix A. Appendix B gives the definitions of the correlation functions and describes the implementation of the cross-correlation function using the segment averaging method. A list of nomenclature is presented in Appendix C.

2. Combining the cross-correlation technique with the analytical model of the fluid-filled pipe

2.1 Introduction

At low frequencies, only a slight difference between the axisymmetric wavenumbers in buried pipes has been found in comparison with the predictions for the fluid-filled pipe *in vacuo* [16]. Thus the analytical model for a fluid-filled pipe *in vacuo*, which simplifies wavenumber predictions of axisymmetric waves is used in this report to study leak detection in buried pipes.

As discussed in Appendix A, each axisymmetric wavenumber can be expressed in terms of a complex wavenumber, the real part of which gives the wavespeed, and the imaginary part of which gives the wave attenuation. The theoretical background of the cross-correlation technique is given in Appendix B. Combining the analytical model of the fluid-borne axisymmetric wave for fluid-filled plastic pipes with the assumption that the leak signal is band-limited white noise, an analytical model of the cross-correlation function is established. The effect of lower and upper cut-off frequencies of the leak signal on the theoretical results is also discussed.

2.2 Theoretical predictions of wavespeed and wave attenuation

Assuming the effect of the $s=2$ axisymmetric wave on the pressure wave motion defined by equation (A.7) is negligible, the internal pressure in the fluid-filled plastic pipe can thus be expressed as a function of time t and distance x by

$$p(x,t) = P_0 e^{i(\omega t - kx)} \tag{2.1}$$

where k is the $s=1$ complex fluid-borne wavenumber given by equation (A.23), which can be expressed as $k = \mathrm{Re}\{k\} + i\,\mathrm{Im}\{k\}$; P_0 is the amplitude of the internal pressure at $x=0$, $t=0$, which is related to equation (A.7) by $P_0 = P_1 J_0\left(k_1' r\right)$. In the case when there is less than one half of a fluid wavelength across the pipe diameter, $P_0 \approx P_1$.

The propagation wavespeed can be obtained from the real part $\mathrm{Re}\{k\}$ by

$$\mathrm{Re}\{k\} = \frac{\omega}{c} \tag{2.2}$$

Assuming that the effect of the wave attenuation on the propagation wavespeed can be ignored, equations (A.23) and (2.2) can be combined to give the theoretical value of the fluid-borne wavespeed

$$c = c_f \left(1 + \frac{2Ba}{Eh}\right)^{-1/2} \tag{2.3}$$

where c_f is the fluid wavespeed. Equation (2.3) indicates that the propagation wavespeed is independent of frequency at low frequencies, which means that wave propagation is non-dispersive at these frequencies.

The imaginary part $\mathrm{Im}\{k\}$ determines the rate of wave attenuation with increasing distance, which is a function of frequency ω,

$$\mathrm{Im}\{k\} = -\beta\omega \tag{2.4}$$

where β is a measure of the loss within the pipe wall. Combining equations (A.23) and (2.4), the theoretical value of the constant β is given by

$$\beta = \frac{1}{c_f} \frac{\frac{\eta Ba}{Eh}}{\left(1 + \frac{2Ba}{Eh}\right)^{1/2}} \tag{2.5}$$

where η is the loss factor of the pipe wall. The loss in dB/m is related to the imaginary part of the wavenumber by

$$Loss = -\frac{20\,\mathrm{Im}\{k\}}{\ln(10)} = -8.67\,\mathrm{Im}\{k\} \tag{2.6}$$

Equation (2.6) shows that there is greater attenuation of waves at high frequencies in fluid-filled plastic pipes, as $\mathrm{Im}\{k\}$ increases with frequency as shown in equation (2.4).

2.3 *Theoretical prediction of the cross-correlation function*

Figure 1 depicts a typical measurement arrangement for a leak in a buried water pipe. The pipe is considered to be anechoic for the fluid-borne wave at all frequencies of interest. Two access points (normally fire hydrants) where sensors can be attached are located on either side of the leak at distance d_1 and d_2. Substituting equations (2.2) and (2.4) into equation (2.1), the pressure in the frequency domain is obtained by

$$p(x,\omega) = P_0(\omega) e^{-i\omega x/c} e^{-\omega\beta x} \tag{2.7}$$

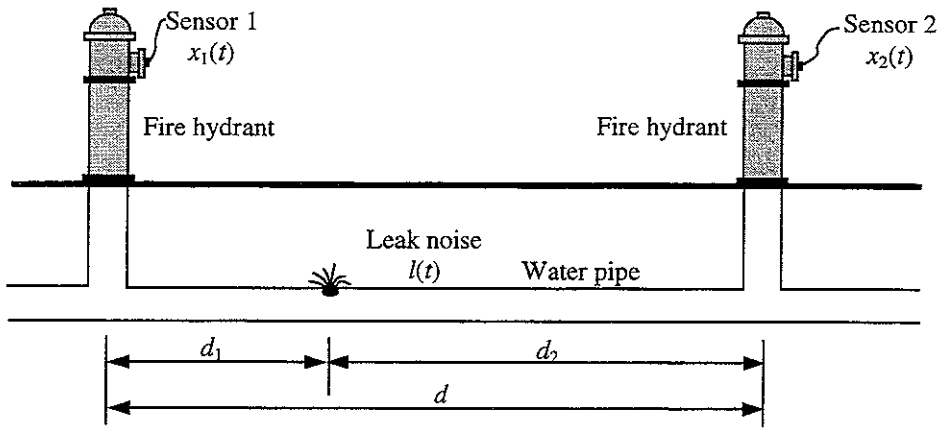

Figure 1. Schematic of a pipe with a leak bracketed by two sensors

The frequency response function between the leak and the sensor signal is given by

$$H(\omega) = \frac{P_0(\omega)e^{-i\omega x/c}e^{-\omega\beta x}}{P_0(\omega)} = e^{-i\omega x/c}e^{-\omega\beta x} \tag{2.8}$$

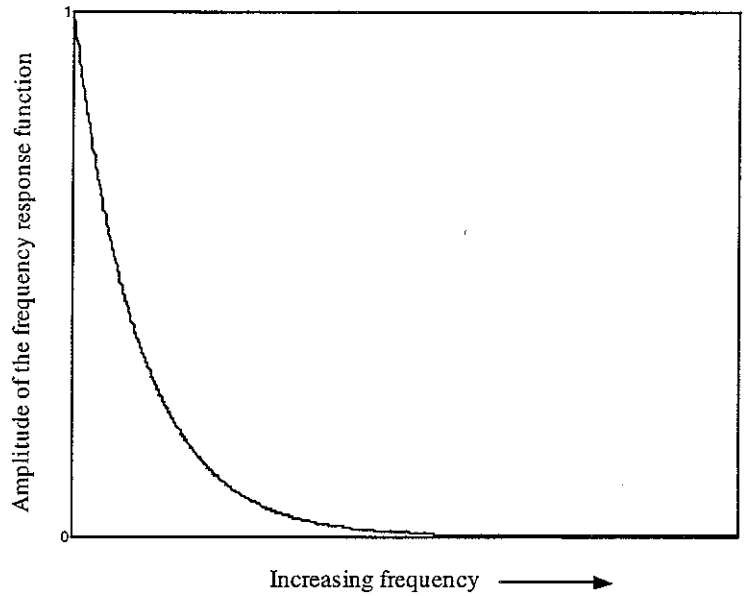

Figure 2. Illustration of the amplitude of the frequency response function

Figure 2 shows that the frequency response function decreases exponentially with increasing frequency. The power spectral densities of the leak signal $S_{LL}(\omega)$ and the sensor signal $S_{XX}(\omega)$ are related to the frequency response function by

$$S_{XX}(\omega) = \lim_{T\to\infty}\frac{E\left[\left|X_T(\omega)\right|^2\right]}{T} = \left|H(\omega)\right|^2 S_{LL}(\omega) \tag{2.9}$$

where $E[\ ]$ is the expectation operator and $X_T(\omega)$ is the Fourier transform of the sensor signal $x(t)$ for time duration T. For two signals measured at positions $x=d_1$ and $x=d_2$, the frequency response function between the positions becomes

$$H(\omega)=\frac{P_0(\omega)e^{-i\omega d_2/c}e^{-\omega\beta d_2}}{P_0(\omega)e^{-i\omega d_1/c}e^{-\omega\beta d_1}}=e^{-i\omega(d_2-d_1)/c}e^{-\omega\beta(d_2-d_1)} \tag{2.10}$$

The corresponding cross-spectral density $S_{X_1X_2}(\omega)$ is defined by

$$S_{X_1X_2}(\omega)=\lim_{T\to\infty}\frac{E\left[X_{1T}^*(\omega)X_{2T}(\omega)\right]}{T}=S_{LL}(\omega)H_1^*(\omega)H_2(\omega) \tag{2.11}$$

where * denotes conjugation; $X_{1T}(\omega)$ and $X_{2T}(\omega)$ are Fourier transforms of the sensor signals $x_1(t)$ and $x_2(t)$ for time duration T; $H_1(\omega)$ and $H_2(\omega)$ are frequency response functions between the leak signal and sensor signals 1 and 2 respectively. Substituting equation (2.8) into equation (2.11) gives

$$S_{X_1X_2}(\omega)=S_{LL}(\omega)\Psi(\omega)e^{-i\omega(d_2-d_1)/c} \tag{2.12}$$

where $\Psi(\omega)=\left|H_1^*(\omega)H_2(\omega)\right|=e^{-\omega\beta(d_2+d_1)}$, which gives the attenuation of the signal with frequency. The phase spectrum of these two signals is dependent on the time shift that the signals experience as they pass through the system, which is given by

$$\Phi_{X_1X_2}(\omega)=Arg\left\{S_{X_1X_2}(\omega)\right\}=-\omega(d_2-d_1)/c \tag{2.13}$$

The cross-correlation function, $R_{x_1x_2}(\tau)$, is related to the cross-spectral density by the inverse Fourier transform

$$R_{x_1x_2}(\tau)=F^{-1}\left\{S_{X_1X_2}(\omega)\right\}=\frac{1}{2\pi}\int_{-\infty}^{+\infty}S_{X_1X_2}(\omega)e^{i\omega\tau}d\omega \tag{2.14}$$

where $F^{-1}\{\ \}$ denotes the inverse Fourier transform. Combining equations (2.12) and (2.14), the cross-correlation function between two sensor signals is determined by

$$R_{x_1x_2}(\tau)=\frac{1}{2\pi}\int_{-\infty}^{+\infty}S_{LL}(\omega)\Psi(\omega)e^{i\omega(\tau+T_0)}d\omega \tag{2.15}$$

where the time shift $T_0=-(d_2-d_1)/c$. Since multiplication in one domain is a convolution in the transformed domain, in terms of the time shift T_0, equation (2.15) can be rewritten as

$$R_{x_1x_2}(\tau)=R_{ll}(\tau)\otimes\psi(\tau+T_0) \tag{2.16}$$

where $\otimes$ denotes convolution; $R_{ll}(\tau)$ is the auto-correlation function of the leak signal; and $\psi(\tau)$ is given by

$$\psi(\tau)=F^{-1}\left\{\Psi(\omega)\right\}=\frac{\beta d}{\pi\left[(\beta d)^2+\tau^2\right]} \tag{2.17}$$

where $d = d_1 + d_2$. Provided that the leak is a white noise signal, the analytical model for the prediction of the cross-correlation function can be obtained. Assuming $S_{LL}(\omega) = S_0$, equation (2.16) becomes

$$R_{x_1x_2}(\tau) = S_0\psi(\tau + T_0) = \frac{S_0\beta d}{\pi\left[(\beta d)^2 + (\tau + T_0)^2\right]} \tag{2.18}$$

By comparing equation (2.12) with equation (2.18), it is clear that the cross-correlation function and the cross-spectral density contain the same information about the time shift between the two sensor signals. The peak value of the correlation function, which occurs at $\tau_{peak} = -T_0 = (d_2 - d_1)/c$, is given by

$$R_{x_1x_2}(\tau_{peak}) = S_0\psi(0) = \frac{S_0}{\pi\beta d} \tag{2.19}$$

The bandwidth of the cross-correlation function $\Delta\tau$ is defined by

$$\frac{R_{x_1x_2}(\tau_{peak} \pm \Delta\tau/2)}{R_{x_1x_2}(\tau_{peak})} = \frac{1}{2} \tag{2.20}$$

Combining equations (2.18), (2.19) and (2.20) gives

$$\Delta\tau = 2\beta d \tag{2.21}$$

It is clear from equations (2.19) and (2.21) that by increasing either the loss (damping) in the pipe wall and/or the distance between the measurement positions of the leak have an effect on the peak value of the correlation function and the width of this peak. To investigate this effect equations (2.19) and (2.21) are normalised so that they can be plotted on a single graph. Combining equations (2.2) and (2.4) gives

$$\hat{\eta} = \frac{-\mathrm{Im}\{k\}}{\mathrm{Re}\{k\}} = \beta c \tag{2.22}$$

In terms of the non-dimensional quantity $\hat{\eta}\dfrac{d}{\sqrt{d_1 d_2}}$, the normalised peak correlation is given by

$$\frac{R_{x_1x_2}(\tau_{peak})\sqrt{\tau_1\tau_2}}{S_0} = \frac{\sqrt{d_1 d_2}}{\pi\hat{\eta}d} \tag{2.23}$$

where $\tau_1 = d_1/c$ and $\tau_2 = d_2/c$. The normalised bandwidth is given by

$$\frac{\Delta\tau}{\sqrt{\tau_1\tau_2}} = 2\hat{\eta}\frac{d}{\sqrt{d_1 d_2}} \tag{2.24}$$

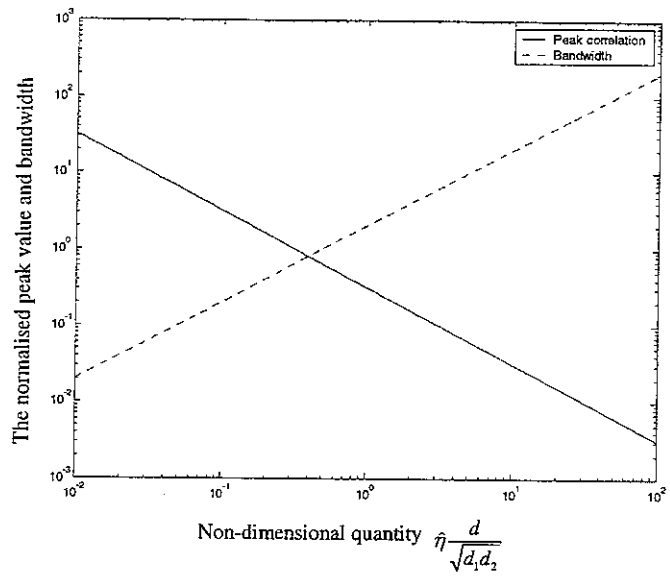

Figure 3. The normalised peak value and bandwidth of the cross-correlation function as a function of the non-dimensional quantify $\hat{\eta}\frac{d}{\sqrt{d_1 d_2}}$

As shown in Figure 3, the normalised peak correlation decreases with increasing $\hat{\eta}\frac{d}{\sqrt{d_1 d_2}}$. This demonstrates that it is more difficult to estimate the time delay from the correlation function if the pipe is heavily damped and/or the measurement position is far from the leak. One the other hand, the correlation function close to the peak value spreads out.

2.4 *Effect of lower and upper cut-off frequencies on the theoretical prediction*

It is emphasised that the frequency response function defined by equation (2.8) is only valid at low frequencies well below the pipe ring frequency. This means that the pressure wave is a non-dispersive propagating wave with a constant attenuation factor β in this frequency range. Therefore it is of interest to investigate the effect of the bandwidth of the leak signal on the theoretical prediction of the cross-correlation function. In this case, the sensor signals are equivalent to passing through an ideal band-pass filter defined as

$$\begin{aligned} G(\omega) &= 1 \qquad \omega_0 \le |\omega| < \omega_1; \\ &= 0 \qquad \text{otherwise.} \end{aligned} \tag{2.25}$$

where ω_0 and ω_1 are the lower and upper cut-off frequencies of the leak signal. Thus the cross-correlation function given by equation (2.18) becomes

$$R_{x_1x_2}(\tau) = S_0\psi^b(\tau + T_0) \tag{2.26}$$

and

$$\begin{aligned}\psi^b(\tau) &= F^{-1}\{\Psi(\omega)G(\omega)\} \\ &= \frac{e^{-\omega_0\beta d}}{\pi\sqrt{(\beta d)^2+\tau^2}}\left[\cos(\omega_0\tau+\theta) - e^{-\Delta\omega\beta d}\cos(\omega_1\tau+\theta)\right]\end{aligned} \tag{2.27}$$

where $\theta = \tan^{-1}\left(\frac{\tau}{\beta d}\right)$ and the frequency bandwidth $\Delta\omega = \omega_1 - \omega_0$. The peak value of the correlation function at $\tau_{peak} = -T_0 = (d_2 - d_1)/c$ is

$$R_{x_1x_2}(\tau_{peak}) = S_0\psi^b(0) = \frac{S_0 e^{-\omega_0\beta d}}{\pi\beta d}\left(1 - e^{-\Delta\omega\beta d}\right) \tag{2.28}$$

Provided that the frequency bandwidth satisfies the condition $e^{-\Delta\omega\beta d} \ll 1$, equation (2.26) can be approximated by

$$R_{x_1x_2}(\tau) = S_0\tilde{\psi}^b(\tau + T_0) \tag{2.29}$$

and

$$\tilde{\psi}^b(\tau) = \frac{e^{-\omega_0\beta d}}{\pi\sqrt{(\beta d)^2+\tau^2}}\cos(\omega_0\tau+\theta) \tag{2.30}$$

Compared with equation (2.27), the interference term caused by the upper cut-off frequency ω_1 does not appear in equation (2.30). Furthermore the difference between equations (2.18) and (2.29) is because of the lower cut-off frequency ω_0. To achieve a large peak value, ω_0 should be as low as possible. Therefore, the cross-correlation function is mainly dominated by the lower cut-off frequency provided that the bandwidth of the input white noise is relatively broad.

2.5 *Theoretical predictions of the cross-correlation coefficient*

As described in Appendix B, it is common practice to express the cross-correlation function in a non-dimensional normalised form, namely the correlation coefficient $\rho_{xy}(\tau)$ defined as

$$\rho_{xy}(\tau) = \frac{R_{xy}(\tau)}{\sqrt{R_{xx}(0)R_{yy}(0)}} \tag{2.31}$$

where $R_{xx}(0)$ and $R_{yy}(0)$ are the values of auto-correlation functions $R_{xx}(\tau)$ and $R_{yy}(\tau)$ at $\tau = 0$. The quantity $\rho_{xy}(\tau)$ can be used to assess the degree of linearity between any two variables x and y on a scale from –1 to +1. It is especially useful when two quantities involved are different in scale and dimension. The auto-correlation function can be derived from the inverse Fourier transform of its auto-spectrum as

$$R_{xx}(\tau) = F^{-1}\{S_{XX}(\omega)\} = \frac{1}{2\pi}\int_{-\infty}^{\infty} S_{XX}(\omega) e^{i\omega\tau} d\omega \tag{2.32}$$

Combining equations (2.8), (2.9) and (2.32), for the band-limited leak noise signal, equation (2.32) can be expressed in terms of a convolution as

$$R_{xx}(\tau) = R_{ll}(\tau) \otimes \varphi^b(\tau) \tag{2.33}$$

and

$$\varphi^b(\tau) = F^{-1}\left\{\left|H(\omega)\right|^2 G(\omega)\right\} = \frac{e^{-2\omega_0\beta x}\cos(\omega_0\tau+\theta) - e^{-2\omega_1\beta x}\cos(\omega_1\tau+\theta)}{\pi\sqrt{(2\beta x)^2+\tau^2}} \tag{2.34}$$

Assuming $S_{LL}(\omega) = S_0$, the maximum value of the auto-correlation function that occurs at $\tau = 0$, is obtained by

$$R_{xx}(0) = S_0\varphi(0) = \frac{S_0 e^{-2\omega_0\beta x}}{2\pi\beta x}\left(1 - e^{-2\Delta\omega\beta x}\right) \tag{2.35}$$

Consider two signals measured at positions $x = d_1$ and $x = d_2$. Combining equations (2.26) and (2.35) gives the normalised cross-correlation function

$$\rho_{x_1x_2}(\tau) = \frac{2\beta\sqrt{d_1 d_2}}{\sqrt{(\beta d)^2 + (\tau+T_0)^2}} \frac{\cos(\omega_0(\tau+T_0)+\theta) - e^{-\Delta\omega\beta d}\cos(\omega_1(\tau+T_0)+\theta)}{\left(1-e^{-2\Delta\omega\beta d_1}\right)^{1/2}\left(1-e^{-2\Delta\omega\beta d_2}\right)^{1/2}} \tag{2.36}$$

At $\tau_{peak} = -T_0 = (d_2 - d_1)/c$, the peak value of the cross-correlation coefficient is

$$\rho_{x_1x_2}(\tau_{peak}) = \frac{2\sqrt{d_1 d_2}}{d} \frac{1-e^{-\Delta\omega\beta d}}{\left(1-e^{-2\Delta\omega\beta d_1}\right)^{1/2}\left(1-e^{-2\Delta\omega\beta d_2}\right)^{1/2}} \tag{2.37}$$

Assuming that $d_1 \approx d_2 \neq 0$, when the frequency bandwidth satisfies $e^{-2\Delta\omega\beta d_1} \ll 1$ (or $e^{-2\Delta\omega\beta d_2} \ll 1$), equation (2.37) gives

$$\rho_{x_1x_2}(\tau_{peak}) = \frac{2\sqrt{d_1 d_2}}{d} \tag{2.38}$$

If d_1 is very small, then $d \approx d_2$. Assume $\Delta\omega$ is still sufficiently large so that $e^{-2\Delta\omega\beta d_2} \ll 1$, but $1-e^{-2\Delta\omega\beta d_1} \approx 2\Delta\omega\beta d_1$. The peak cross-correlation coefficient given by equation (2.37) becomes

$$\rho_{x_1x_2}(\tau_{peak}) = \sqrt{\frac{2}{\beta d_2 \Delta\omega}} \tag{2.39}$$

Similarly when d_2 is very small, the peak cross-correlation coefficient is given by

$$\rho_{x_1x_2}(\tau_{peak}) = \sqrt{\frac{2}{\beta d_1 \Delta\omega}} \tag{2.40}$$

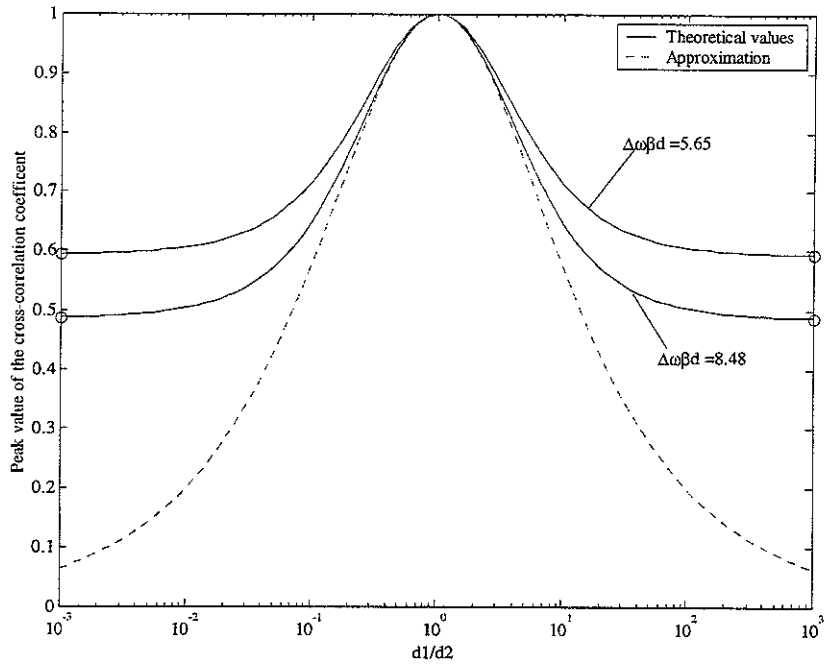

Figure 4. Peak value of the cross-correlation coefficient as a function of the ratio of the distances d_1 and d_2

The comparison of the peak cross-correlation coefficient given by equation (2.37) and its approximation by equation (2.38) is shown in Figure 4. As the product $\Delta\omega\beta d$ increases, the theoretical value approaches the approximation. The two points marked by 'o' are given by equations (2.39) and (2.40), which provide the approximate peak value of the cross-correlation coefficient as one sensor is moved close to the leak. For two equispaced sensors $d_1/d_2 = 1$, the peak cross-correlation coefficient is found to be unity, which simply means there is a perfect linear relationship between these two sensor signals. In comparison with the theoretical value, good agreement can always be achieved when $d_1/d_2 \approx 1$.

2.6 *Summary*

Combining the analytical model of fluid-filled pipes discussed in Appendix A, theoretical predictions of propagation wavespeed and wave attenuation have been studied in this section. Assuming that the leak signal is band-limited white noise, an analytical model of the cross-correlation function has been established. Several expressions for the theoretical predictions of cross-correlation functions including the cross-correlation coefficient have been derived. The effect of lower and upper cut-off frequencies of the leak signal on the theoretical results have also been discussed. It has been found that the cross-correlation function is mainly dominated by the lower cut-off frequency provided that the bandwidth of the input white noise is relatively broad.

3. Validation of analytical models

3.1 Introduction

The analytical models established in section 2 are assessed to identify their effectiveness so that they could be applied to leak detection in plastic pipes. Experimental results provided by the National Research Council of Canada are analysed in this section. The normalised cross-correlation functions of the data measured are calculated by using the segment averaging method described in Appendix B. The effect of lower and upper cut-off frequencies on the cross-correlation function is taken into account using a digitised filter with different band-pass frequencies.

3.2 Brief description of the sensor signals

The description of the test site and measurement procedures are detailed in reference [7]. A joint leak signal was measured by hydrophones and accelerometers. The hydrophones were attached to two fire hydrants, while accelerometers were located underground attached to shut-off values near the fire hydrants. Referring to Figure 1, the distance d between the two sensor signals was 102.6m, and the distance d_1 from the leak to sensor 1 was 73.5m. The signals were first passed through an anti-aliasing filter with the cut-off frequency set at 200Hz. A 66-second segment of hydrophone-measured signals were then digitised at a sampling frequency of 500 samples/second. The same sampling frequency was applied to the accelerometer-measured signals for the time duration of 60 seconds.

3.3 Results and discussions

3.3.1 Validation of theoretical predictions of wavespeed and attenuation for the fluid-borne axisymmetric wave

Spectral analysis was performed on the digitised data using a 1024-point FFT, Hanning window with 40% overlap and power spectrum averaging. The following observations [7] are based on the auto-spectra and coherence functions of sensor signals measured by both hydrophones and accelerometers as plotted in Figure 5.

- Below 5Hz it is believed that the signals were dominated by ambient noise at peaks corresponding to the longitudinal resonance frequencies of the test pipe.
- The coherence function between accelerometer-measured signals was much poorer than that between hydrophone-measured signals. A reasonable

explanation is perhaps that acceleration signals were dominated by incoherent noise, which was easily diminished by spectral averaging.

- ❖ Most of the frequency content of sensor signals for both hydrophone and accelerometer-measured signals was concentrated below 50Hz.
- ❖ Anomalous peaks in the auto-spectra of the two sensor signals are found at different frequencies due to several sources including longitudinal resonance of the water pipe, soil resonance, or fundamental frequencies of rotating machinery on the test site, etc.

Although the tests were carried out at the experimental site where PVC pipes were buried in soft clay soil, the effect of the surrounding medium on the wavenumber prediction is relatively small at frequencies well below the pipe ring frequency [16]. Equations (2.2) and (2.4) can thus be used to predict wavespeed and attenuation respectively.

The axisymmetric wavespeed can be determined from either the frequency response function between two sensor signals or the corresponding cross-spectral density. The same information about the relative phase angle between two sensor signals is provided by these two quantities, which can be seen from equations (2.10) and (2.13). In practice, due to the presence of significant amounts of background noise, smoothing operations must be performed before determining the phase angle. The relative phase angle obtained from the hydrophone and accelerometer-measured signals is shown in Figures 5a, b (iv).

Since generally there is more than half a wavelength between the sensor signals, the phase angle displayed in the range $\pm 180^{\circ}$ must be unwrapped. The unwrapped phase angle is related to the wrapped relative phase by adding an appropriate integer number of 180° as follows

when n is an odd,

$$\alpha = 180(n+1) - \alpha_{wrap} \tag{3.1}$$

when n is a even,

$$\alpha = 180n + \alpha_{wrap} \tag{3.2}$$

where α, α_{wrap} are the unwrapped and wrapped phase angle in degree respectively.

The corresponding unwrapped phase angle is plotted in Figure 6. For hydrophone-measured signals, a straight line indicates that the wavespeed is independent of

frequency below 150Hz. Similarly a linear dependence was found roughly below 140Hz for accelerometer-measured signals. However, they did not go through the origin. This was possibly caused by the dominant ambient noise at low frequencies. The least square fit line was also plotted by selecting several points marked on each unwrapped phase angle.

The propagation wavespeed can be determined from the unwrapped relative angle by

$$c = \frac{360(d_1 - d_2)f}{\alpha} \tag{3.3}$$

where f is the frequency in Hz.

Based on the slope of the least square fit line plotted in Figure 6, the wavespeed calculated is 478m/s and 480m/s for hydrophone and accelerometer-measured signals respectively. Good agreement has been achieved compared with the results obtained in previous work [17]. This validates the value of the fluid-borne axisymmetric wavespeed predicted by the analytical model.

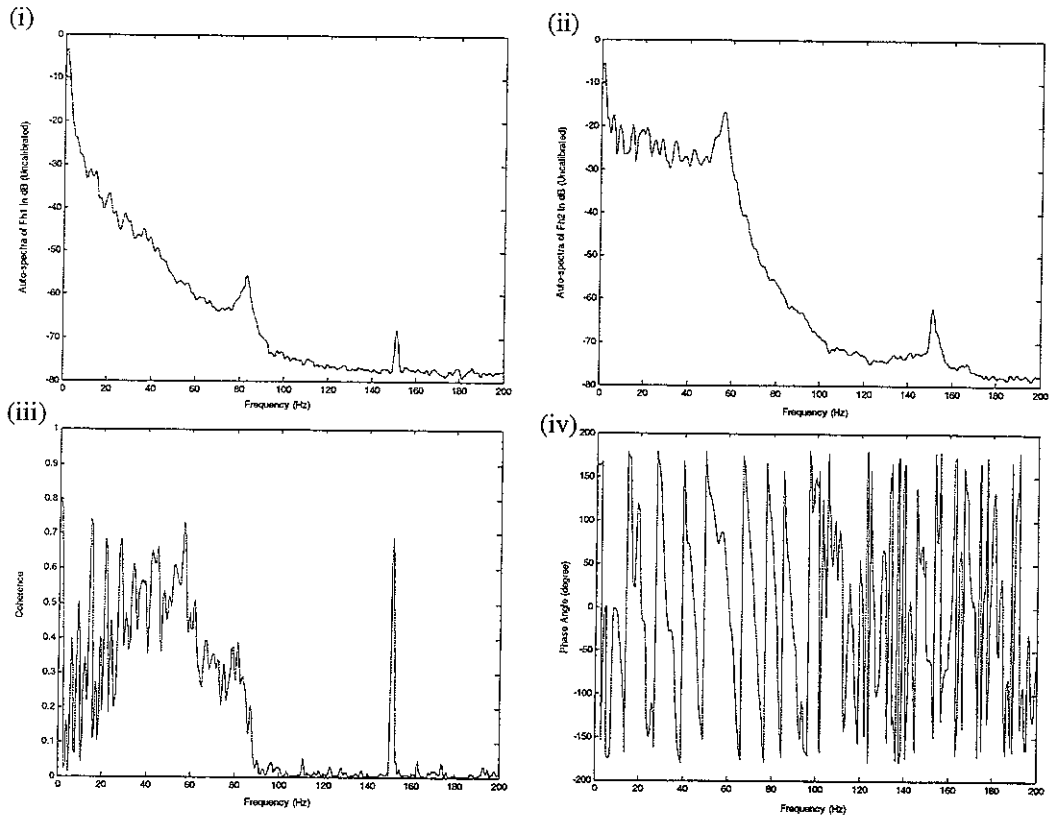

(a) Hydrophone-measured signals

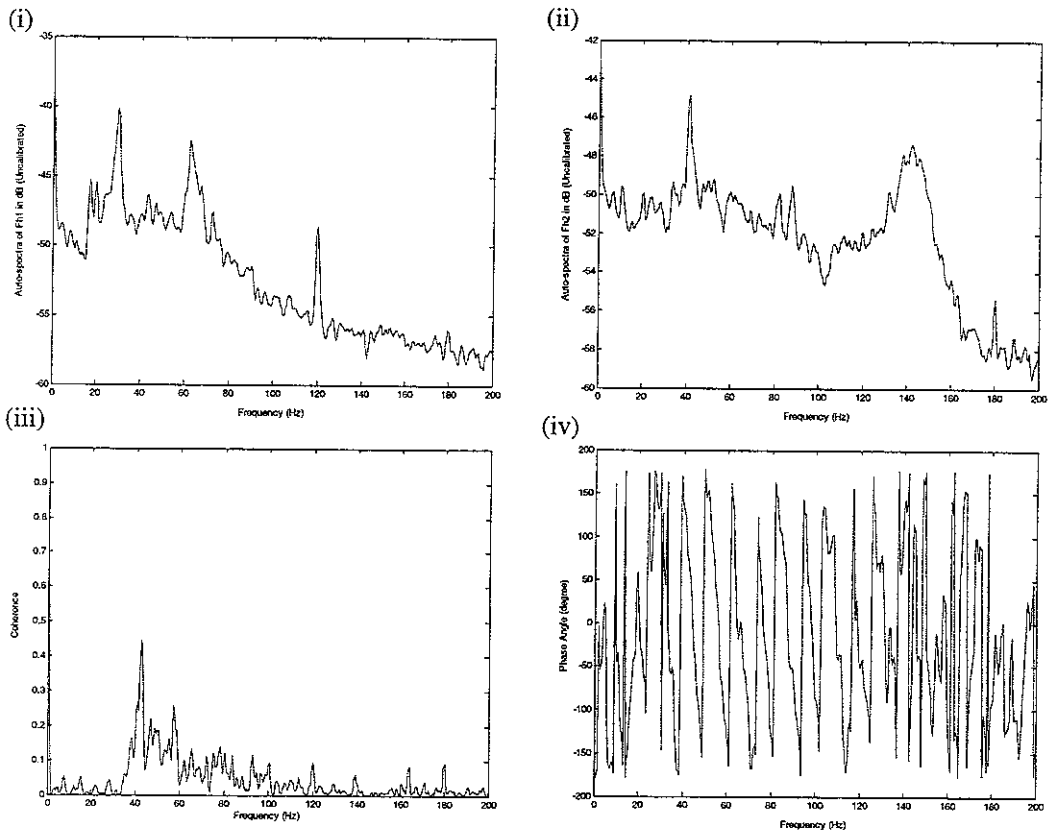

(b) Accelerometer-measured signals

Figure 5. Comparison of the auto-spectra, coherence and phase spectra of sensor signals measured by hydrophones and accelerometers: (i) Auto-spectrum of sensor signal 1; (ii) Auto-spectrum of sensor signal 2; (iii) Coherence function; (iv) Phase angle in degrees.

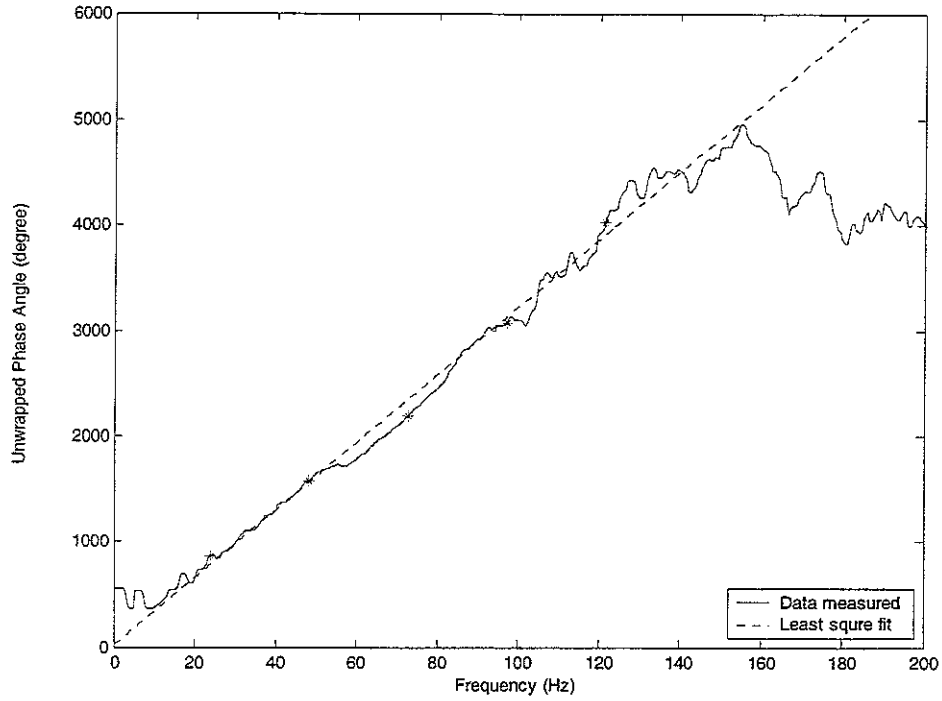

(a) Hydrophone-measured signals

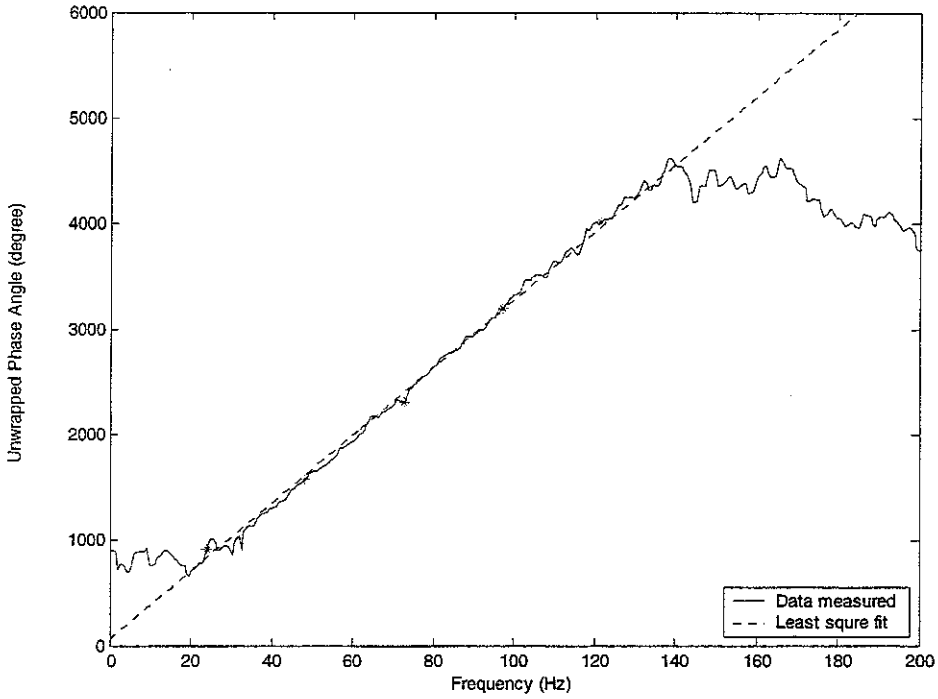

(b) Accelerometer-measured signals

Figure 6. Unwrapped phase angle between two sensor signals

The wave attenuation can be derived from the amplitude of the frequency response function between the two sensor signals. Combing equations (2.4), (2.6) and (2.10), the loss in dB/m is related to the frequency response function by

$$Loss = \frac{-20\ln|H(\omega)|}{\Delta d \ln(10)} \tag{3.4}$$

where $|H(\omega)|$ denotes the amplitude of the frequency response function between the two sensor signals and the distance difference $\Delta d = d_2 - d_1$.

The amplitudes of the frequency response functions calculated from data measured by two types of sensors are plotted in Figure 7. Deviations of the frequency response function from the mean value were relatively large for both hydrophone and accelerometer-measured signals. For hydrophone-measured signals, the linear relationship of the amplitude of the frequency response function in dB with frequencies below 50Hz validates the theoretical prediction of the wave attenuation presented in section 3. The corresponding least square fit line gives the attenuation factor β of 8.95e-5 s/m and the non-dimensional quantity $\hat{\eta} = \beta c = 0.0428$. However the analytical model failed to analyse the amplitude of the frequency response function obtained from accelerometer-measured signals.

Figure 8 illustrates the loss in dB/m as a function of frequency based on equation (3.4). The loss derived from hydrophone-measured data confirms that the loss within the pipe increases with increasing frequencies at low frequencies below 50Hz. However the low-frequency behaviour of accelerometer-measured signals was puzzling. It seems that there was little wave attenuation below 80Hz, which was not predicted by the analytical model.

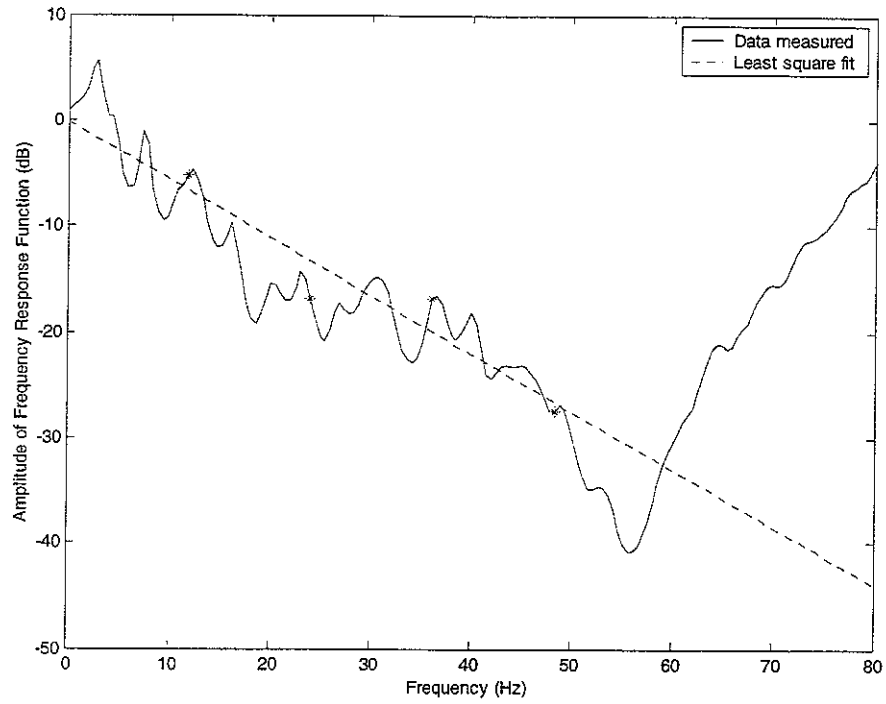

(a) Hydrophone-measured signal

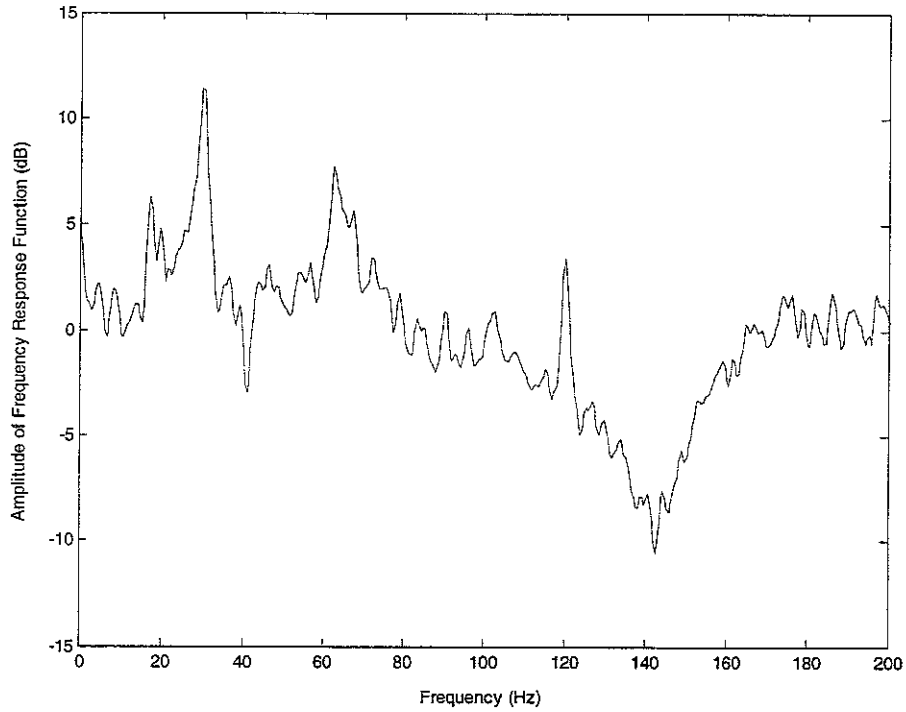

(b) Accelerometer-measured signals

Figure 7. Comparison of the amplitudes of the frequency response functions derived from: (a) Hydrophone-measured signals; (b) Accelerometer-measured signals.

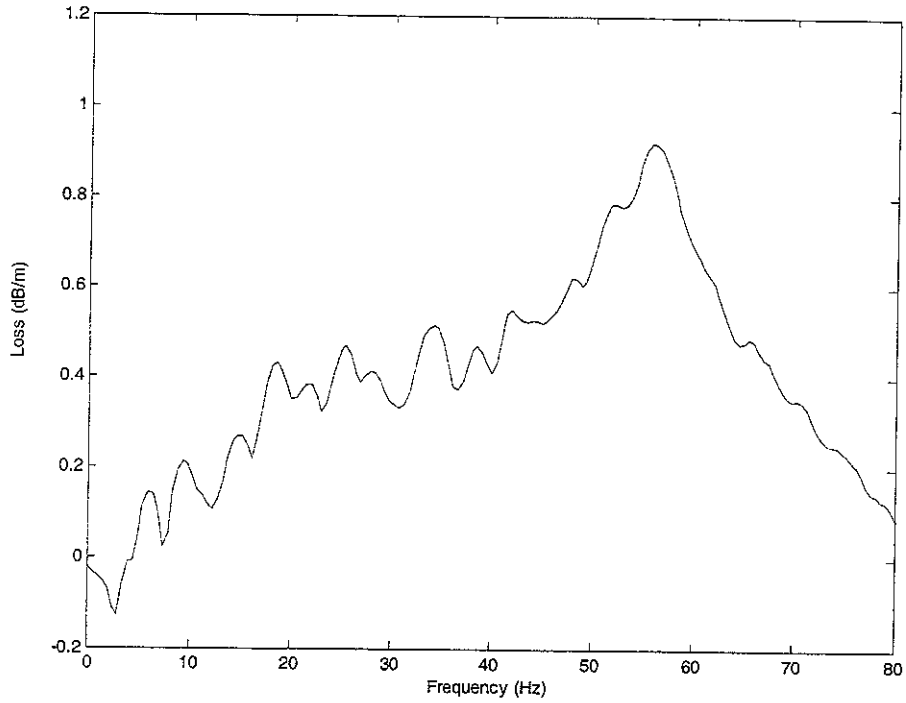

(a) Hydrophone-measured signals

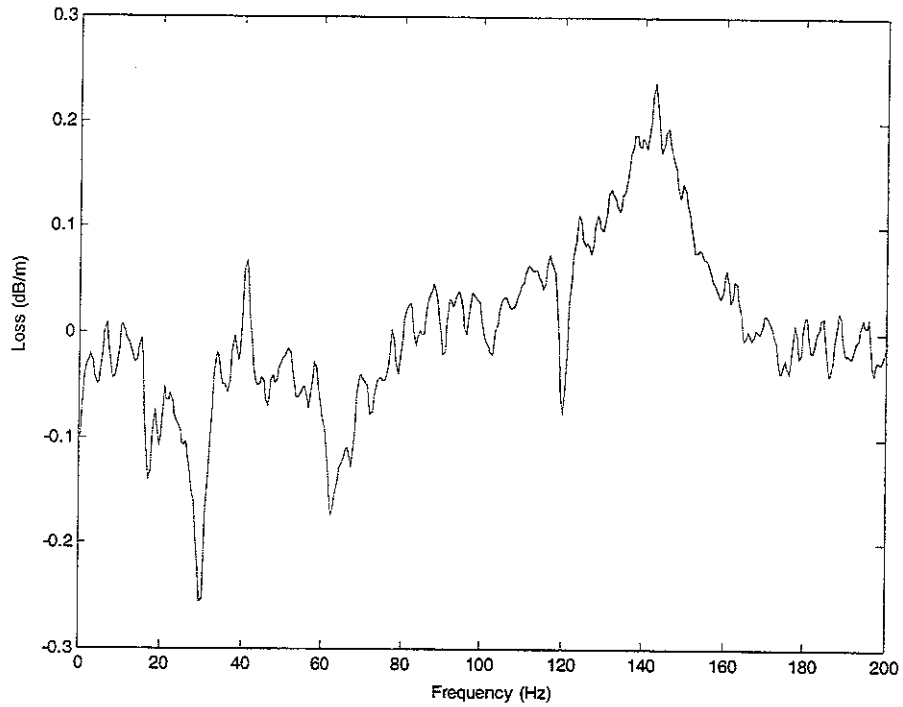

(b) Accelerometer-measured signals

Figure 8. Comparison of loss in dB/unit distance calculated from
(a) Hydrophone-measured signals; (b) Accelerometer-measured signals.

3.3.2 *Analysis of sensor signals by using the cross-correlation method*

Assuming that a leak exists between the two points where two sensors are attached, a distinct peak can be found in the cross-correlation function and the corresponding time delay, τ_{peak}, shows the difference in arrival times between two sensor signals. With reference to Figure 1, the time delay is related to the locations of the sensors by

$$\tau_{peak} = \frac{d_2 - d_1}{c} \tag{3.5}$$

By substituting $d_2 = d - d_1$ into the above equation, the position of the leak relative to sensor 1 is found to be

$$d_1 = \frac{d - c\tau_{peak}}{2} \tag{3.6}$$

where the distance between the two sensors, d, usually measured on site or read off system maps. The propagation wavespeed, c, can be obtained from pipe manufacturers or is easily measured on-site using a known in-bracket or out-of-bracket simulated leak.

As mentioned above, below 5Hz the signals were dominated by ambient noise at peaks corresponding to the longitudinal resonance frequencies of the test pipe. Therefore filtering operations must be performed on the digitised sensor signals before conducting the time domain cross-correlation. The main procedures of the cross-correlation analysis were performed as follows:

(1) The digitised sensor signals were first passed through high and low-pass filters of the 4th order Butterworth type;

(2) The normalised cross-correlation functions were computed by using segment averaging via a 1024-point FFT. The circular effect implicit in the FFT was eliminated by 50% zero padding in each segment record.

From equation (2.11), the leak spectrum can be reconstructed by

$$S_{LL}(\omega) = \frac{S_{X_1X_2}(\omega)}{H_1^*(\omega)H_2(\omega)} \tag{3.7}$$

where $S_{X_1X_2}(\omega)$ is the measured cross-spectrum between the two sensor signals; $H_1(\omega)$ and $H_2(\omega)$ are the predicted frequency response functions using the analytical model. As shown in Figure 9, a relatively 'flat' leak spectrum was found in the frequency range from 5Hz to 50Hz. The variance of this estimation was very large due to unpredictable ambient noise, soil properties and the pipe wall itself. For

hydrophone-measured signals, the effect of the low-pass filter cut-off frequency on the normalised cross-correlation function is shown in Figure 10. The cut-off frequencies were set at 10Hz for high-pass filters, while changing the cut-off frequencies from 30Hz to 200Hz for low-pass filters. It was found in section 3 that the effect of the upper cut-off frequency is negligible provided that the pass band of the leak signal is relatively broad. This effect can easily be seen from Figures 10 (a)-(c), because there was not a large difference in the normalised cross-correlation functions when the low-pass filters were set from 30Hz to 50Hz. Furthermore, when the low-pass filter cut-off frequencies were set above 50Hz, the correlation functions plotted in Figures 10 (d)-(f) resembled each other and the peak correlation values were slightly changed. The similarity indicates that most information about the leak signal was concentrated below 50Hz. It can be seen from Figure 9 that the ambient noise was predominantly measured by the hydrophones above 50Hz. Thus for the hydrophone-measured signals, the correlation technique is suggested to be applied in the range from 5Hz to 50Hz.

Comparison of normalised cross-correlation functions calculated from the original signal and theoretical value is made in Figure 11. The cut-off frequencies of the low-pass filters were 50Hz and those of the high-pass filters were set from 5Hz to 40Hz. For comparison, the normalised cross-correlation functions obtained from accelerometer-measured signals are plotted in Figure 12. Several main findings and observations are as follows:

- For the correlation functions derived from the original hydrophone-measured signals as shown in Figure 11 (a), a definite peak was obtained although the oscillation behaviour of the correlation function became more obvious as the pass band of the leak signal became smaller in the frequency domain. The time delay was estimated to be in the range 0.090~0.094s and the position of the leak relative to point 1 was calculated to be 72.8-73.8m. Furthermore, as expected, a definite peak could not always be obtained when the cut-off frequency of the high-pass filter was set below 5Hz due to the dominant ambient noise.
- The theoretical values of the normalised cross-correlation functions were improved significantly compared with the experimental results. The reason of their difference was due to the effect of the background noise on the sensor

signals measured. In terms of the cut-off frequencies of the digital filters, the same oscillation behaviour of the correlation coefficient could be found as the results calculated from the hydrophone-measured signals.

- Compared with the hydrophone-measured signals, the correlation functions obtained from accelerometer-measured signals produced a more pronounced peak despite the poorer coherence between the signals measured. The normalised correlation functions obtained from hydrophone-measured signals were nearly twice as large as those for accelerometer-measured signals. A distinct peak could be found by correlating the accelerometer-measured signals without a digital filter as shown in Figure 12 (a).
- Referring to Figure 6 (b), for the accelerometer-measured signals a linear dependence was found below 140Hz. Thus, the sensor signals were passed through the digital filters with the cut-off frequencies set at 30Hz and 140Hz respectively. Similar to the hydrophone-measured signals, the high-pass filter removed the effect of the ambient noise below 30Hz. The normalised correlation function is plotted in Figure 12 (b). Compared with Figure 12 (a), the peak correlation value was improved by using digital filters. Moreover, as shown in Figure 12 (c), when the pass band of the leak signal was much broader, the peak value could not be enhanced. It indicates that the correlation technique was most effectively performed in the frequency band from 30Hz to 140Hz. The relative distance d_1 was 72.9~73.4m, which could be determined from the time delay in the range 0.090~0.092s.

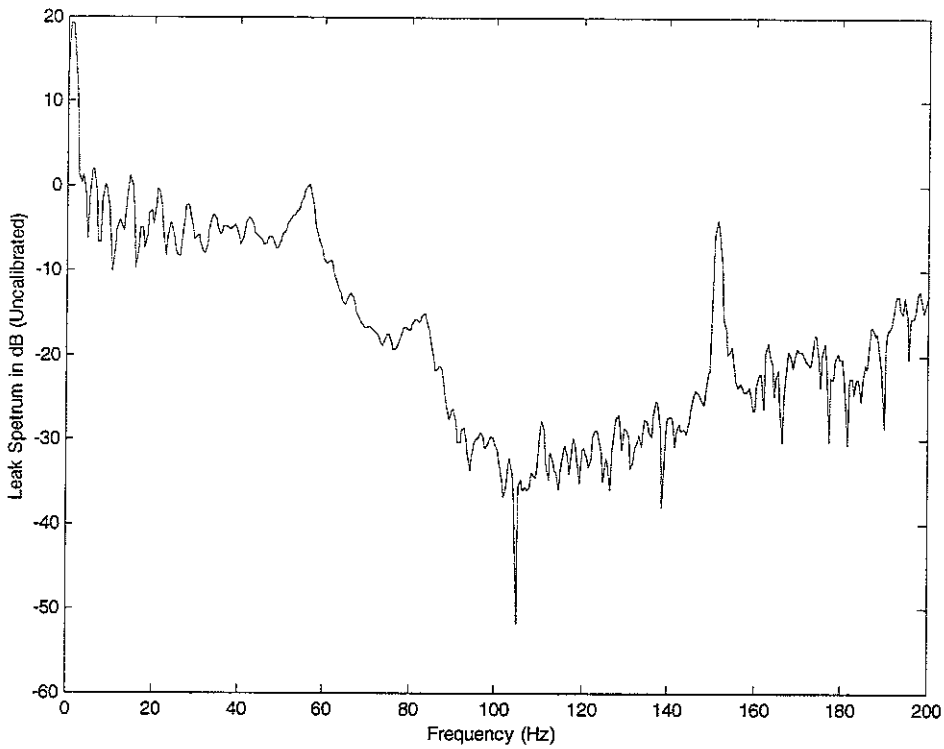

Figure 9. Leak spectrum reconstructed from the cross-spectrum between hydrophone-measured signals

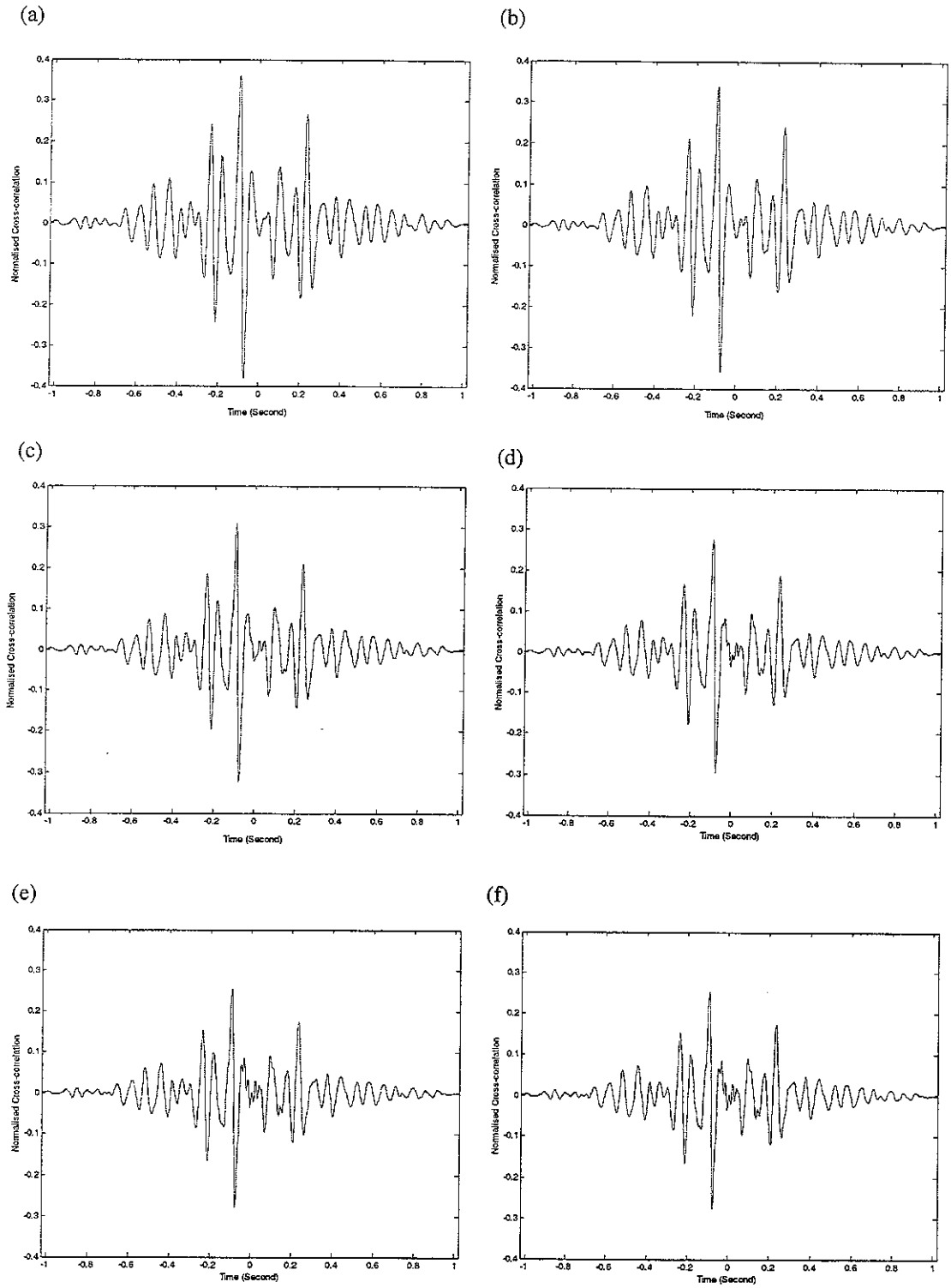

Figure 10. Effect of the low-pass filter cut-off frequency on the normalised cross-correlation function for hydrophone-measured data. The cut-off frequencies of high-pass filters are set at 10Hz.

The low-pass filter cut-off frequencies are:

(a) 30Hz; (b) 40Hz; (c) 50Hz; (d) 60Hz; (e) 100Hz; (f) 200Hz.

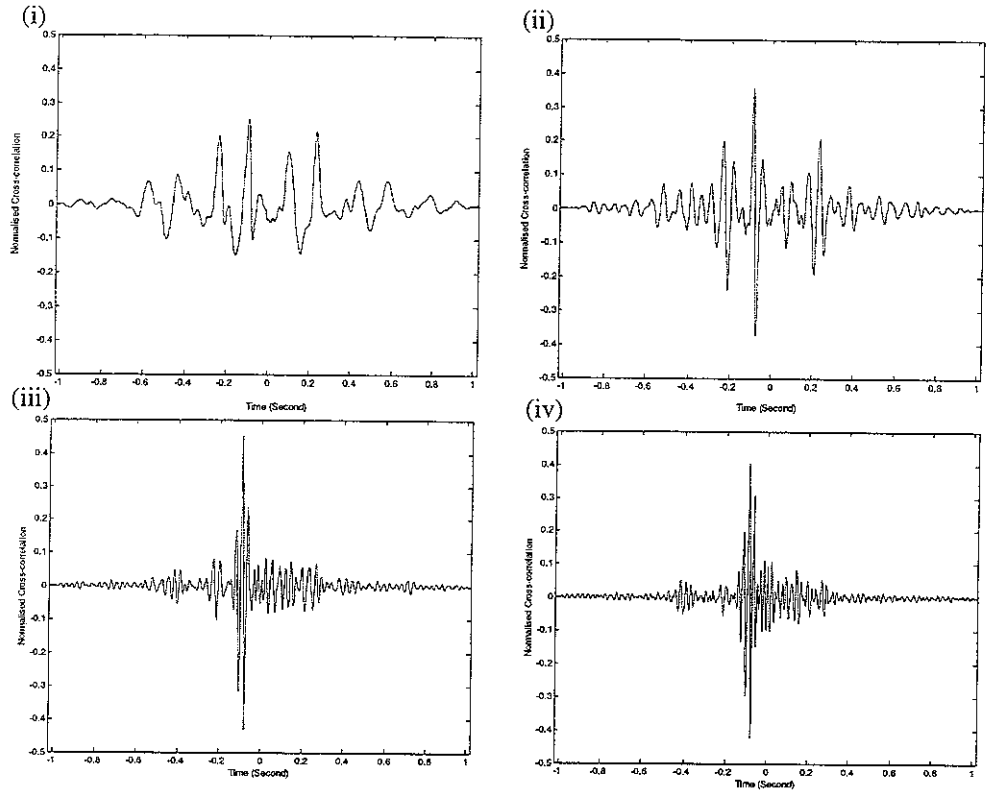

(a) Original hydrophone-measured data

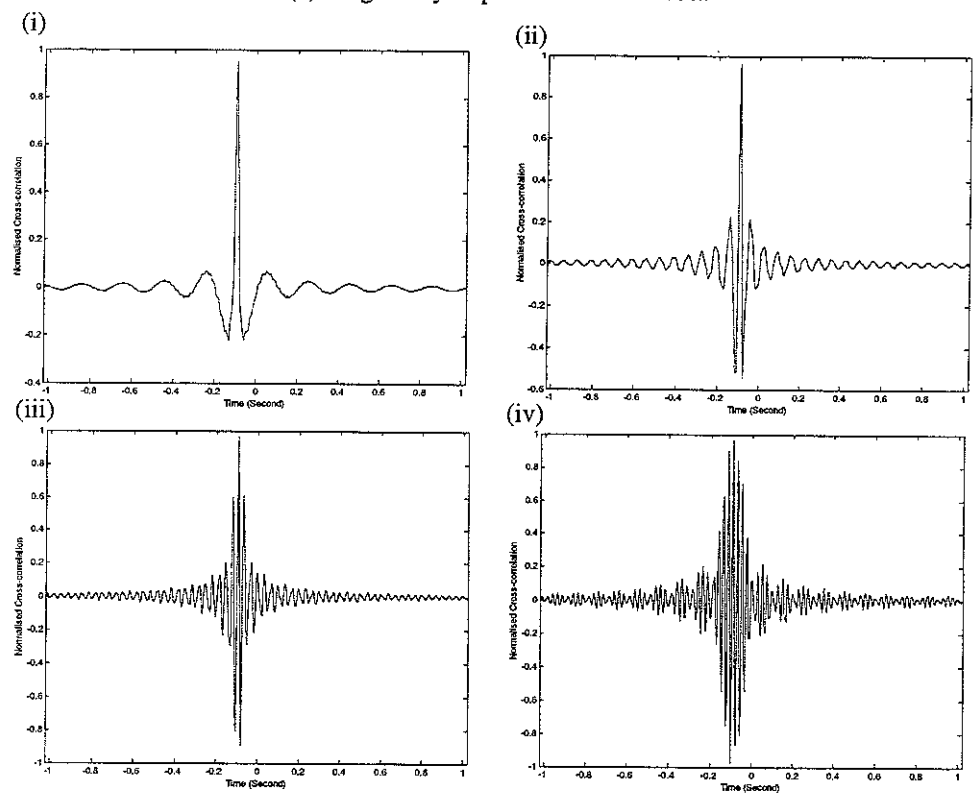

(b) Theoretical values

Figure 11 Effect of the high-pass filter cut-off frequency on the normalised cross-correlation function for hydrophone-measured data. The cut-off frequencies of low-pass filters are set at 50Hz.

The low-pass filter cut-off frequencies are: (a) 5Hz; (b) 15Hz; (c) 30Hz; (d) 40Hz.

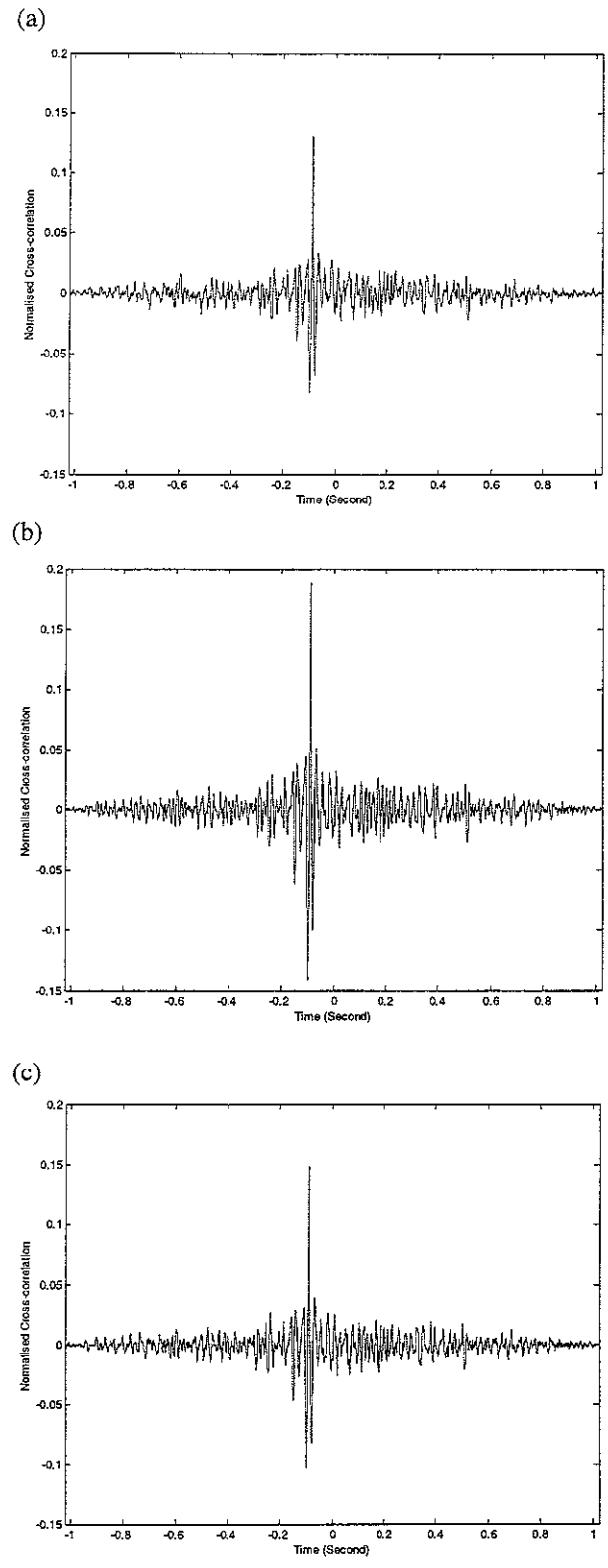

Figure 12. The normalised cross-correlation functions for accelerometer-measured signals: (a) without a filter; (b) using digital filters with the cut-off frequencies set at 30Hz and 140Hz; (c) using digital filters with the cut-off frequencies set at 20Hz and 200Hz.

3.4 Summary

The analytical models established in section 2 have been evaluated in this section. Compared with the results obtained by the National Research Council of Canada [17], good agreement has been achieved in the analysis of the propagation wavespeed. The theoretical prediction of wave attenuation was proved by analysing hydrophone-measured data. However the analytical model failed in the analysis of the accelerometer-measured signals.

The normalised cross-correlation functions obtained from both hydrophone and accelerometer-measured data were performed by using the segment averaging method. For the hydrophone-measured signals, the effect of the lower and upper cut-off frequencies on the cross-correlation function was investigated by using digital filters with different cut-off frequencies. In addition, the assumption of the model presented in the previous section was validated by the leak spectrum reconstructed. The model of the correlation function provides a reasonable explanation for the effect of the filter cut-off frequencies on the cross-correlation technique.

Although the model was not valid for the accelerometer-measured signals, the normalised correlation function could be improved if the cut-off frequencies of the digital filters were properly selected.

4. Conclusions

The existing leak detection techniques and equipment have been reviewed in this report. The analytical models of leak detection for plastic pipes by using the correlation technique have been established. The main findings can be summarised as follows:

- An analytical model of the propagation wavespeed and wave attenuation has been established. It has been validated by analysing the experimental results provided by the National Research Council of Canada.
- Assuming that the leak signal is band-limited white noise, an analytical model of the cross-correlation function has been established. Several expressions for theoretical predictions of cross-correlation functions have been derived. It has been found that cross-correlation functions are mainly dominated by the lower cut-off frequency provided that the bandwidth of the input white noise is relatively broad. Regarding the normalised cross-correlation functions calculated from the experimental data, the model presented is found to provide a reasonable explanation for the effect of the filter cut-off frequencies on the cross-correlation technique for leak detection.
- The dynamic behaviour of a fluid-filled pipe *in vacuo* has been reviewed in Appendix A. For plastic pipes, it is found that the fluid-borne ($s=1$) axisymmetric wave is strongly influenced by the pipe wall flexibility. The effect of the $s=2$ wave on the pressure and radial wave motions for the water-filled pipe can be neglected.

Acknowledgements

The authors gratefully acknowledge the support of Osama Hunaidi, the National Research Council of Canada in supplying data from their experimental work on leak detection.

Appendix A: Dynamic behaviour of fluid-filled pipes

A.1 Introduction

The objective of this appendix is to review the low-frequency behaviour of fluid-filled pipes. The characteristics of wave propagation in buried pipes have been discussed by Muggleton et al [16]. They found that at low frequencies the effect of the surrounding medium on the axisymmetric wavenumbers is relatively small compared to the results for the fluid-filled pipe *in vacuo*. Therefore an analytical model for a fluid-filled pipe *in vacuo* developed by Pinnington and Briscoe [14] is discussed in this appendix. This model is based on simplified Kennard's equations [18], which neglect pipe bending, transverse shear and rotary inertia in the pipe wall.

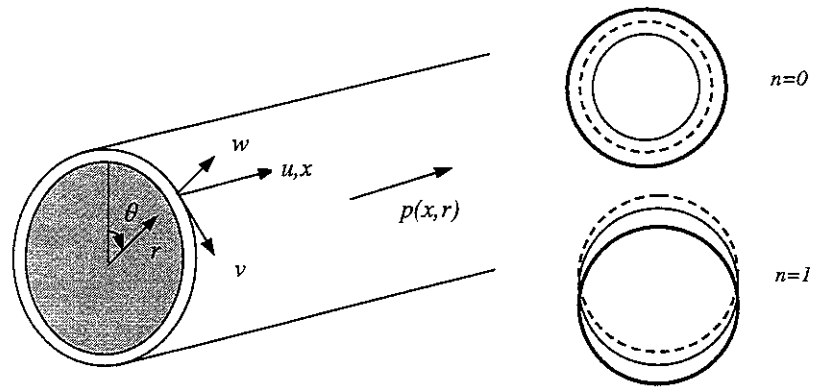

Figure A1. The coordinate system for a fluid-filled pipe and modal shapes

The mode shapes and coordinate system for the pipe considered are illustrated in Figure A1. The two frequency regimes of a fluid-filled pipe are separated by the pipe ring frequency, ω_0, which is the frequency at which the pipe shell vibrates in a "breathing" ($n=0$) mode and occurs when the circumference of the pipe equals to a compressional wavelength [19]. Well below the pipe ring frequency, four wave types are considered to be responsible for most of the energy transfer [9, 14]. These are three axisymmetric waves associated with the $n=0$ mode, and the wave related to beam bending ($n=1$). Two of the axisymmetric waves involve both structural and fluid motion, and the strength of the coupling between these motions is governed by the dimensions of the pipe and its physical properties. The third wave is a torsional wave in the shell uncoupled from the contained fluid and does not have significant radial motion. The $n=1$ bending wave is a beam-like flexural wave and consists of near-field and dispersive propagating waves with the cross-section of the pipe remaining

largely undeformed. Above the pipe ring frequency, the dynamic behaviour of fluid-filled pipes is much more complicated and is not considered here.

This appendix reviews the pipe equations for axisymmetric wave motions consisting of the $s=1$ and $s=2$ waves for a fluid-filled pipe *in vacuo* derived in reference [14]. The contributions of each axisymmetric wave for the plastic pipe are given in terms of the relative size of the relationships between internal pressure and radial wall motions.

A.2 Equations of motion

The co-ordinate system for the fluid-filled semi-infinite cylindrical shell is shown in Figure A1. x, θ and r are the axial, circumferential and radial coordinates respectively; u, v and w are the shell displacements in these directions. (A list of nomenclature is given in Appendix C.) The pipe has a mean radius a and wall thickness h, which satisfies the condition $h/a \ll 1$. The following equations are simplified forms of Kennard's equations for a thin-walled shell [18], with shell bending neglected, and so are only valid below the pipe ring frequency.

Equilibrium of forces in the axial direction gives

$$\rho \ddot{u} = \partial \sigma_x / \partial x \tag{A.1}$$

Assuming no circumferential variation, equilibrium of forces in the radial direction leads to

$$p(a/h) = \sigma_\theta + \rho a \ddot{w} \tag{A.2}$$

The Hooke's Law relationships for the shell are [20]

$$\sigma_x = \frac{E}{1-\nu^2}\left(\frac{\partial u}{\partial x} + \nu \frac{w}{a}\right) \tag{A.3}$$

$$\sigma_\theta = \frac{E}{1-\nu^2}\left(\frac{w}{a} + \nu \frac{\partial u}{\partial x}\right) \tag{A.4}$$

where $\frac{w}{a}$ and $\frac{\partial u}{\partial x}$ are the circumferential and axial strains. Substituting equation (A.3) into equation (A.1) gives

$$\rho \ddot{u} - \frac{E}{1-\nu^2}\left(\frac{\partial^2 u}{\partial^2 x} + \frac{\nu}{a}\frac{\partial w}{\partial x}\right) = 0 \tag{A.5}$$

Similarly equations (A.2) and (A.4) give

$$\frac{E}{1-\nu^2}\left(\frac{w}{a} + \nu \frac{\partial u}{\partial x}\right) + \rho a \ddot{w} = \frac{pa}{h} \tag{A.6}$$

These are two coupled equations for the axiymmetric wave motion. Travelling wave solutions of the form $u = \sum_{s=1}^{2} U_s e^{i(\omega t - k_s x)}$ and $w = \sum_{s=1}^{2} W_s e^{i(\omega t - k_s x)}$ may be used to describe the displacement variations in time and space.

The internal pressure can be described by a Bessel function of order zero,

$$p = \sum_{s=1}^{2} P_s J_0(k_s^r r) e^{i(\omega t - k_s x)} \tag{A.7}$$

where the radial wavenumber, k_s^r, is related to the fluid wavenumber, k_f, by

$$(k_s^r)^2 = k_f^2 - k_s^2 \tag{A.8}$$

Substitution of these displacement and pressure solutions into equations (A.5) and (A.6) gives the following relationship for the $s = 1$ and $s = 2$ wavenumbers

$$(k_L^2 a^2 - k_s^2 a^2) U_s = i\nu k_s a W_s \tag{A.9}$$

$$W_s(1 - k_L^2 a^2) - i\nu k_s a U_s = P_s J_0(k_s^r a) a^2 \frac{(1-\nu^2)}{Eh} \tag{A.10}$$

where k_L is the wavenumber of a compressional wave in a plate, which is given by $k_L^2 = \omega^2 \rho \frac{(1-\nu^2)}{E}$.

Each of pressure waves must have a radial displacement at the boundary $r = a$, which is equal to the shell displacement. For each wave mode the radial velocity of the fluid at the shell wall, given by the fluid momentum equation, is

$$v_r\big|_{r=a} = -\left(\frac{1}{i\rho_f \omega}\right) \partial p / \partial r \tag{A.11}$$

Equations (A.7) and (A.11) can be combined to give

$$v_r\big|_{r=a} = -\frac{k_s^r J_0'(k_s^r a)}{i\rho_f \omega} P_s e^{i(\omega t - k_s x)} \tag{A.12}$$

where a prime denotes differentiation with respect to the argument $k_s^r r$. Equating v_r to the shell radial velocity, which is derived from the differentiation of the shell displacement in the radial direction with respect to time, enables the fluid pressure amplitude to be written in terms of the shell radial displacement amplitude as

$$P_s = \frac{\omega^2 \rho_f}{k_s^r J_0'(k_s^r a)} W_s \tag{A.13}$$

For small arguments, where there is less than one half of a fluid wavelength across the pipe diameter, $J_0'(k_s' a) \approx -\frac{k_s' a}{2}$. The small argument approximation for the Bessel functions may be applied to equation (A.13), which gives

$$P_s = \frac{-2B}{1-\left(\frac{k_s}{k_f}\right)^2}\frac{W_s}{a} \tag{A.14}$$

Combining equations (A.9), (A.10) and (A.14) gives the following relationship for the axisymmetric wavenumbers

$$1-k_L^2 a^2 + \frac{\nu^2 k_s^2}{k_L^2 - k_s^2} + \frac{\gamma k_f^2}{k_f^2 - k_s^2} = 0 \tag{A.15}$$

where γ is fluid loading term due to pressure of the fluid acoustic field, which is given by

$$\gamma = \frac{2Ba(1-\nu^2)}{Eh} \tag{A.16}$$

A.3 Wavenumber predictions of axiymmetric waves

Equation (A.15) can be used to determine the axiymmetric wavenumbers. The $s=1$ (the predominantly fluid-borne wave) wavenumber can be found by assuming $k_s^2 \gg k_L^2$, that is, the wavespeed of the $s=1$ wave is much slower than the plate compressional wavespeed. The solution for the $s=1$ wave is given by

$$k_1^2 = k_f^2\left(1+\frac{\gamma}{1-\nu^2-\Omega^2}\right) \tag{A.17}$$

where the normalised ring frequency $\Omega = k_L a$, which is the ratio of the excitation frequency to the pipe ring frequency. It can be seen that the $s=1$ axisymmetric wave is always slower than the wave in an infinite medium with a wavenumber k_f.

The solution for the $s=1$ wave can be reformulated in terms of the impedance of the contained fluid, z_{fluid}, and the pipe wall impedance, z_{pipe}, as

$$k_1^2 = k_f^2\left(1+\frac{z_{fluid}}{z_{pipe}}\right) \tag{A.18}$$

where $z_{fluid} = -2iB/a\omega$ and $z_{pipe} = z_{Mpipe} + z_{Kpipe} = i\left(\rho h\omega - Eh/a^2\omega\right)$.

At low frequencies, $\Omega \ll 1$, the contribution of the pipe wall inertia term, z_{Mpipe}, is relatively small compared with the pipe wall stiffness term, z_{Kpipe}. Equation (A.18) thus becomes

$$k_1^2 = k_f^2\left(1+\frac{2Ba}{Eh}\right) \tag{A.19}$$

In the case when the contained fluid is water, for the same size of pipe, the $s=1$ wavenumber is determined by the material property of the pipe wall. For a plastic pipe wall, for example typical PVC pipe with $a/h=10$, $E=5\times10^9\text{N/m}^2$, $k_1 \approx 3.2k_f$. For an even softer pipe wall, the $s=1$ wavenumber is much greater than the wavenumber in the infinite medium. This indicates that the wavespeed of the fluid-borne wave for the plastic pipe decreases rapidly with increasing fluid loading (decreasing pipe wall stiffness).

As for the $s=2$ wave (the axial shell wave), the wavenumber can be obtained with the knowledge that it is always smaller than the fluid wavenumber k_f. Setting $k_s^2 \ll k_f^2$, the solution for the $s=2$ wave can be found from equation (A.15)

$$k_2^2 = k_L^2\left(\frac{1}{1-\dfrac{\nu^2}{1-\Omega^2+\gamma}}\right) \tag{A.20}$$

Similarly equation (A.20) can be reformulated in terms of the impedance of the contained fluid, z_{fluid}, the pipe wall impedance, z_{pipe}, and the impedance of the pipe wall stiffness, z_{Kpipe}, as

$$k_2^2 = k_L^2\left(1+\frac{\nu^2}{1-\nu^2}\frac{z_{Kpipe}}{z_{pipe}+z_{fluid}}\right) \tag{A.21}$$

At low frequencies, $\Omega \ll 1$, the contribution of the pipe mass term is negligible, the solution for the $s=2$ wavenumber becomes

$$k_2^2 = k_L^2\left(1+\frac{\nu^2}{1-\nu^2}\frac{1}{1+\dfrac{2Ba}{Eh}}\right) \tag{A.22}$$

It is clear that the $s=2$ axisymmetric wave is slower than the compressional wave in a plate, k_L, well below the pipe ring frequency. Thus the wavenumber k_2 satisfies the

relationship $k_L^2 < k_2^2 \ll k_f^2$. For the PVC pipe discussed above, it is found that the $s=2$ wavespeed is very close to the compressional wavespeed k_L. In fact, the wavespeed of the $s=2$ wave can be considered to be equal to the plate compressional wavespeed for most plastic pipes. As the plate compressional wavenumber is comparable to the fluid wavenumber, the wavenumber k_2 is not substantially smaller than the fluid wavenumber k_f as expected.

In practice the pipe wall material itself is always lossy, and the loss within the pipe wall may be represented by a complex elastic modulus, $E(1+i\eta)$. The complex axisymmetric wavenumbers can also be derived by equations (A.18) and (A.21). However, in this case the impedance of the pipe wall stiffness is given by $z_{Kpipe} = -\frac{iEh}{a^2\omega} + \frac{\eta Eh}{a^2\omega}$. Particularly at low frequencies, equations (A.19) and (A.22) becomes

$$k_1^2 = k_f^2\left(1+\frac{2Ba}{Eh+i\eta Eh}\right) \tag{A.23}$$

and

$$k_2^2 = k_L^2\left(1+\frac{\nu^2}{1-\nu^2}\frac{1}{\left(1+\frac{2Ba}{Eh}\right)-\frac{2iBa}{\eta Eh}}\right) \tag{A.24}$$

A.4 *Relationship between the internal pressure and radial wall motions*

The relationship between the internal pressure and radial wall motions for the two axisymmetric waves is found by substituting equations (A.17) and (A.20) into equation (A.14). For the $s=1$ wave,

$$W_1 = \left(\frac{1}{1-\frac{\Omega^2}{1-\nu^2}}\right)\frac{P_1 a^2}{Eh} \tag{A.25}$$

For the $s=2$ wave,

$$W_2 = -\frac{P_2 a}{2B} \tag{A.26}$$

These equations can be combined to give the ratio of radial wave motions for the two wave types in terms of the ratio of the pressure waves

$$\frac{W_1}{W_2} = \frac{-\gamma}{1-\nu^2-\Omega^2}\frac{P_1}{P_2} \tag{A.27}$$

At low frequencies, the ratio can be reduced to

$$\frac{W_1}{W_2} = \frac{-\gamma}{1-\nu^2}\frac{P_1}{P_2} \tag{A.28}$$

For most practical pipework systems these two wave types are strongly coupled. In this circumstance it is of interest to know the expected ratio of radial wall motions associated with these two waves. Assuming the two modal energies are the same, the ratio of radial wall motions at low frequencies is found to be given approximately by [14]

$$\left|\frac{W_2}{W_1}\right|^2 \approx \frac{k_2}{k_1}\frac{\nu^2}{(1+\gamma)\gamma} \tag{A.29}$$

Substituting into equation (A.28) gives the ratio of pressure waves

$$\left|\frac{P_2}{P_1}\right|^2 \approx \frac{k_2}{k_1}\frac{\nu^2}{\left(1-\nu^2\right)^2}\frac{\gamma}{1+\gamma} \tag{A.30}$$

For soft-walled pipes, that is, the Young's modulus of the shell is comparable with the fluid bulk modulus ($\gamma \gg 1$), equation (A.30) can be further approximated by

$$\left|\frac{P_2}{P_1}\right| \approx \frac{\nu}{1-\nu^2}\sqrt{\frac{k_2}{k_1}} \tag{A.31}$$

Considering the PVC pipe mentioned previously with $a/h = 10$, $\gamma = 7.6$, the ratios of pressure and radial waves given by equations (A.31) and (A.29) are both 0.03. Thus for the water-filled pipe with higher fluid loading, the effect of the $s = 2$ wave on the pressure and radial wave motions can be neglected.

A.5 Summary

The wavenumbers of two axisymmetric waves for a fluid-filled pipe *in vacuo* have been reviewed in this appendix. For plastic pipes, it is found that the $s = 1$ axisymmetric wave is strongly influenced by the pipe wall flexibility. However, the $s = 2$ wave is slightly influenced by the contained fluid. The contributions of each axisymmetric wave have been discussed in terms of the relative size of the relationships between the internal pressure and radial wall motions. Consequently, the

effect of the $s = 2$ wave on the pressure and radial wave motions for the water-filled pipe can be neglected.

Appendix B: Implementation of the cross-correlation function using the segment averaging method

In this appendix the implementation of the cross-correlation function using segment averaging via the FFT is presented. It is first necessary to recall the definitions of correlation functions. Consider the situation where the data of interest are two continuous random process $x(t)$ and $y(t)$, which are assumed to be stationary (ergodic). Setting the mean value of each process is zero, the cross-correlation function is defined by

$$R_{xy}(\tau) = E\left[x(t)y(t+\tau)\right] \tag{B.1}$$

where τ is the lag of time; $E[\ ]$ is the expectation operator.

The normalized (non-dimensional) form of the cross-correlation function, sometimes called the correlation coefficient, is given by

$$\rho_{xy}(\tau) = \frac{R_{xy}(\tau)}{\sqrt{R_{xx}(0)R_{yy}(0)}} \tag{B.2}$$

where $R_{xx}(0)$ and $R_{yy}(0)$ are the values of auto-correlation functions $R_{xx}(\tau)$ and $R_{yy}(\tau)$ at $\tau = 0$. The auto-correlation function for a random process $x(t)$ is defined as

$$R_{xx}(\tau) = E\left[x(t)x(t+\tau)\right] \tag{B.3}$$

The normalised form of the auto-correlation function is

$$\rho_{xx}(\tau) = \frac{R_{xx}(\tau)}{R_{xx}(0)} \tag{B.4}$$

From their definitions, the properties of correlation functions [21] are detailed as follows,

For the auto-correlation function

(I) $R_{xx}(\tau)$ is always an even function of τ, that is, $R_{xx}(\tau) = R_{xx}(-\tau)$.

(II) $R_{xx}(\tau)$ attains its maximum value at zero lag, namely, $\left|R_{xx}(\tau)\right| \le R_{xx}(0)$.

(III) Evaluating the auto-correlation function at zero lag gives the variance of the process, that is, $R_{xx}(0) = \sigma_x^2$.

(IV) $R_{xx}(\tau)$ collapses to zero which is the square of the mean value of the process $x(t)$ as τ increases.

(V) The normalized auto-correlation function satisfies: $-1 \le \rho_{xx}(\tau) \le 1$, and $\rho_{xx}(0) = 1$.

For the cross-correlation function

(I) The cross-correlation function is neither an even nor an odd function of τ, but satisfies the relation: $R_{xy}(\tau) = R_{yx}(-\tau)$.

(II) The cross-correlation function follows $|R_{xy}(\tau)| \le \sqrt{R_{xx}(0)R_{yy}(0)}$, which is commonly called the cross-correlation inequality.

(III) Unlike the auto-correlation function, $R_{xy}(0)$ is not the maximum value of $R_{xy}(\tau)$. In addition, $R_{xy}(0)$ has no specific relationship to the variance of the process.

(IV) The normalized cross-correlation function satisfies: $-1 \le \rho_{xy}(\tau) \le 1$.

B.1 Correlation function estimators

When computing the correlation functions from a time series, one assumes ergodicity and uses a time average. If two random signals $x(t)$ and $y(t)$ are defined in the common time interval $0 \le t \le T$, two commonly used estimators of the theoretical cross-correlation function are derived, which can be written as $\hat{R}_{xy}(\tau)$ and $\tilde{R}_{xy}(\tau)$ respectively. The biased estimator $\hat{R}_{xy}(\tau)$ is given by

$$\begin{aligned} \hat{R}_{xy}(\tau) &= \frac{1}{T}\int_0^{T-\tau} x(t)y(t+\tau)dt \qquad \tau > 0 \\ \hat{R}_{xy}(\tau) &= \frac{1}{T}\int_{T+\tau}^{T} x(t)y(t+\tau)dt \qquad \tau < 0 \end{aligned} \tag{B.5}$$

The unbiased estimator $\tilde{R}_{xy}(\tau)$ is given by

$$\begin{aligned} \tilde{R}_{xy}(\tau) &= \frac{1}{T-\tau}\int_0^{T-\tau} x(t)y(t+\tau)dt \qquad \tau > 0 \\ \tilde{R}_{xy}(\tau) &= \frac{1}{T-|\tau|}\int_{T+\tau}^{T} x(t)y(t+\tau)dt \qquad \tau < 0 \end{aligned} \tag{B.6}$$

Both of these two estimators are used for engineering problems because they have intuitive appeals and should be compared on the basis of some criteria [21].

B.2 Computation of the cross-correlation function using sampled data

The procedures for implementation of the cross-correlation function using sampled data are detailed in this section. Assuming both x_n and y_n are N-point sequences, the method of calculation using the biased estimator defined by equation (B.5) is

$$\hat{R}_{xy}(m) = \frac{1}{N}\sum_{n=0}^{N-1-m} x_n y_{n+m}$$
$$\hat{R}_{xy}(-m) = \frac{1}{N}\sum_{n=0}^{N-1-m} y_n x_{n+m} \qquad (m>0;\ n=0,1,...,N-1) \tag{B.7}$$

A similar method can be used to derive the unbiased estimator. These expressions are the so-called 'mean lagged product' formulae and are evaluated directly if the signals are not very long time series. Although equation (B.7) provides the most direct method of estimating the correlation function, it turns out that the frequency domain implementation via the FFT is generally more efficient to evaluate the correlation function indirectly.

One way to reduce the tedious computation, at the expense of some loss of accuracy, is to use segment averaging. The time averaged correlation function as defined by equation (B.7) is very closely related to convolution. In fact $\sum_{n=0}^{N-1-m} x_n y_{n+m}$ can be regarded as a convolution of $x(n)$ with $y(-n)$. Thus the required correlation function can be derived from the inverse FFT of $X^*(k)Y(k)$ and scaled appropriately. Here $X^*(k)$ denotes the complex conjugation of the FFT of $x(n)$; $Y(k)$ is the FFT of $y(n)$.

In conclusion, the approach to implementing the estimation of the cross-correlation function for digital signals can be obtained by the following process:

(1) Fourier transform $x(n)$ and $y(n)$ using the FFT to give $X(k)$ and $Y(k)$;

(2) Form the product of $X^*(k)Y(k)$;

(3) Inverse FFT of $X^*(k)Y(k)$.

However when computing the correlation function of a very long time series, even using the FFT can be computationally demanding. Based on the frequency domain implementation using the FFT method, segment averaging can be applied further to reduce the computational load as follows:

(1) The data is divided into small slices of the same time length;

(2) Estimate the cross-correlation function of each slice via the FFT.

(3) Average all the estimates.

When this method is applied, one has to ensure that the segment length is significantly longer than any delays that may exist between the two signals.

Appendix C: Nomenclature

x, θ, r	axial, circumferential and radial directions
u, v, w	shell displacements in the axial, circumferential and radial directions
v_r	radial velocity of the fluid
σ_x, σ_θ	axial and circumferential normal stress
a, h	pipe radius, wall thickness
ρ, ρ_f	shell, fluid density
E, ν	Young's modulus, Poisson ratio of shell material
B	fluid bulk modulus of elasticity
p	fluid pressure
U_s, W_s	amplitudes of axial and radial displacements of the s wave
P_s	pressure amplitude of the s wave
k_s	axial wavenumber of the s wave
k_f	freefield fluid wavenumber
k_L	axial wavenumber of a compressional wave in a plate of the shell thickness
k_s^r	radial wavenubmer for the s wave in contained media
γ	fluid loading term
Ω	normalised frequency which is given by $\Omega = k_L a$
c_f	wavespeed in an infinite medium
η	loss factor of the pipe wall

References

1. M. Fantozzi, G. D. Chirico, E. Fontana, and F. Tonolini, *Leak inspection on water pipelines by acoustic emission with cross-correlation method.* Annual Conference Proceeding, American Water Works Association, Engineering and Operations, 1993: p. 609-721.
2. H. V. Fuchs and R. Riehle, *Ten years of experience with leak detection by acoustic signal analysis.* Applied Acoustics, 1991. **33**(1): p. 1-19.
3. D. A. Liston and J. D. Liston, *Leak detection techniques.* Journal of the New England Water Works Association, 1992. **106**(2): p. 103-108.
4. G. J. Weil, *Non contact, remote sensing of buried water pipeline leaks using infrared thermography.* Water Resources Planning and Management and Urban Water Resources, 1993: p. 404-407.
5. K. W. Sneddon, G. R. Olhoeft, and M. H. Powers, *Determining and mapping DNAPL saturation values from noninvasive GPR measurements.* Proc. of SAGEEP 2000, 2000: p. 293-302.
6. O. Hunaidi, *Ground-penetrating radar for detection of leaks in buried plastic water distribution pipes.* Seventh International Conference on Ground-Penetrating Radar, 1998: p. 783-786.
7. O. Hunaidi, W. Chu, A. Wang, and W. Guan, *Detecting leaks in plastic pipes.* Journal American Water Works Association, 2000. **92**(2): p. 82-94.
8. G. D. Tattersall and P. W. Linford, *WITE project final workshop document.* 2001: University of East Anglia.
9. C. R. Fuller and F. G. Fahy, *Characteristics of wave propagation and energy distributions in cylindrical elastic shells filled with fluid.* Journal of Sound and Vibration, 1982. **81**: p. 501-518.
10. C. R. Fuller, *The input mobility of an infinite circular cylindrical elastic shell filled with fluid.* Journal of Sound and Vibration, 1983. **87**: p. 409-427.
11. A. W. Leissa, Vibration of Shells, NASA SP-288, 1973(Washington, D. C: Scientific and technical information office, NASA).
12. P. Esparcieux, *Measurement of vibrational wave characteristics of beams and pipes with and without discontinuity.* PhD Thesis, University of Southampton, 1986.

13. C. R. Fuller, *The input mobility of an infinite circular cylindrical shell fitted with fluid.* Journal of Sound and Vibration, 1987: p. 409-427.
14. R. J. Pinnington and A. R. Briscoe, *Externally applied sensor for axisymmetric waves in a fluid filled pipe.* Journal of Sound and Vibration, 1994. **173**(4): p. 503-516.
15. J. M. Muggleton, M. J. Brennan, and R. J. Rinnington, *Development of a Water Pipe Monitoring System for Leak Detection: Experimental Work.* Technical Memorandum No. 860, 2001.
16. J. M. Muggleton, M. J. Brennan, and R. J. Pinnington, *Wavenumber prediction of waves in buried pipes for water leak detection.* Journal of Sound and Vibration, 2002. **249**(5): p. 934-954.
17. O. Hunaidi and W. T. Chu, *Acoustical characteristics of leak signals in plastic water distribution pipes.* Applied Acoustics, 1999. **58**(3): p. 235-254.
18. E. H. Kennard, *The new approach to shell theory: circular cylinders.* Journal of Applied Mechanics, 1953: p. 33-40.
19. M. J. Brennan, S. J. Elliott, and R. J. Pinnington, *A non-intrusive fluid-wave actuator and sensor pair for the active control of fluid-borne vibrations in a pipe.* Smart Materials & Structures, 1996. **5**(3): p. 281-296.
20. W. Flügge, *Stress in shells.* Springer Verlag, Berlin, 1973.
21. J. S. Bendat and A. G. Piersol, Engineering of applications of correlation and spectral analysis, 1993.